Thermal Instability of Cycled $Li_xNi_{0.5}Mn_{0.5}O_2$ Electrodes: An in Situ Synchrotron X-ray Powder Diffraction Study

Naoaki Yabuuchi, Yong-Tae Kim, Hayley H. Li, and Yang Shao-Horn*

Department of Mechanical Engineering, Massachusetts Institute of Technology, Cambridge, Massachusetts 02139

Received January 30, 2008. Revised Manuscript Received April 14, 2008

Thermal instability of pristine $LiNi_{0.5}Mn_{0.5}O_2$ powder and cycled $Li_xNi_{0.5}Mn_{0.5}O_2$ electrodes in the charged ($x = 0.2$) and discharged ($x = 0.9$) states (without electrolyte) was studied by in situ synchrotron powder X-ray diffraction and thermogravimetric analysis (TGA) in the temperature range from 25 to 600 °C in inert atmosphere. Neither structural change nor oxygen loss was found in rhombohedral layered $LiNi_{0.5}Mn_{0.5}O_2$ upon heating to 600 °C. $Li_xNi_{0.5}Mn_{0.5}O_2$ electrodes were found to retain the rhombohedral, layered structure with space group $R\bar{3}m$ until the temperature reached ~300 °C (~275 °C for $Li_{0.2}Ni_{0.5}Mn_{0.5}O_2$ and ~350 °C for $Li_{0.9}Ni_{0.5}Mn_{0.5}O_2$). Rietveld refinement revealed that a considerable amount of octahedral cations migrated from the transition metal layer to the Li layer in the rhombohedral structure of $Li_{0.2}Ni_{0.5}Mn_{0.5}O_2$ from 100 to 275 °C while no detectable change in the cation distribution was noted for $Li_{0.9}Ni_{0.5}Mn_{0.5}O_2$ up to 300 °C. TGA results showed that the weight loss from $Li_{0.2}Ni_{0.5}Mn_{0.5}O_2$ and $Li_{0.9}Ni_{0.5}Mn_{0.5}O_2$ began at ~260 °C and ~400 °C, respectively, and considerably higher weight loss was found for $Li_{0.2}Ni_{0.5}Mn_{0.5}O_2$ relative to $Li_{0.9}Ni_{0.5}Mn_{0.5}O_2$ upon heating. The thermal decomposition of charged $Li_{0.2}Ni_{0.5}Mn_{0.5}O_2$ was found to occur at ~300 °C and to include the following processes: (1) the formation of a spinel-type structure ($Fd\bar{3}m$) at ~300 °C, which was shown present between 300 °C and 600 °C, and (2) the formation of a rocksalt-type phase ($Fm\bar{3}m$) at ~500 °C, which was shown to be present between 500 °C and 600 °C. In addition to these two phase transitions, recrystallization of a rhombohedral phase (having unit cell dimensions similar to those of pristine $LiNi_{0.5}Mn_{0.5}O_2$ but with considerably more interlayer mixing of Li and transition metal ions) was observed upon heating $Li_{0.9}Ni_{0.5}Mn_{0.5}O_2$ to 600 °C, which was accompanied with the appearance of Ni metal. The onset temperatures of structural transitions to the spinel-type and rocksalt-type structures from $Li_{0.2}Ni_{0.5}Mn_{0.5}O_2$ were ~100 °C and ~230 °C higher than those previously reported for Li_xNiO_2 ($x = 0.3$) measured under similar conditions in previous studies, respectively.

Introduction

Recent research focuses on the development of large-scale lithium-ion batteries for hybrid electric vehicle and electric vehicle applications. Although high power and high energy are highly desirable performance characteristics, safety is one of the most important considerations in these applications. Thermal stability of lithium storage materials with and without the presence of electrolyte plays an important role in the lithium battery safety characteristics. Li_xNiO_2 is a high-energy[1–4] electrode material, but its poor thermal stability in the charged state limits its practical use, especially in large-scale battery systems. Substitution of electrochemically inactive cations such as Al^{3+} has shown to improve the thermal stability of $Li_xAl_yNi_{1-y}O_2$.[5–7] Differential scanning calorimetry (DSC) measurements have shown that substitution of 0.25 nickel ions per formula unit by aluminum ions, that is, $Li_xAl_{1/4}Ni_{3/4}O_2$, reduces the rate and amount of heat generated from the exothermic reaction associated with charged electrodes in the presence of electrolyte.[5] However, aluminum substitution reduces rechargeable capacities of $Li_xAl_yNi_{1-y}O_2$[7] as Al^{3+} in the layered structure is not electrochemically active. For example, $Li_xNi_{1.02}O_2$ shows a rechargeable capacity of ~175 (mA h)/g in the voltage range of 2.5−4.15 V while $Li_xAl_{0.16}Ni_{0.89}O_2$ exhibits 125 (mA h)/g under the same condition.[7] Recently researchers have shown that substitution of 0.5 Ni ions per formula unit by Mn in the solid matrix ($LiNi_{0.5}Mn_{0.5}O_2$) not only results in significantly improved thermal stability in comparison to Li_xNiO_2 electrodes[8–12] but also provides excellent reversible capacities on the order of 200 (mA h)/g upon charging to 4.6 V.[8,12–17]

* Corresponding author. E-mail: shaohorn@mit.edu.

(1) Ohzuku, T.; Ueda, A.; Nagayama, M. *J. Electrochem. Soc.* **1993**, *140*, 1862.
(2) Li, W.; Reimers, J. N.; Dahn, J. R. *Solid State Ionics* **1993**, *67*, 123.
(3) Peres, J. P.; Delmas, C.; Rougier, A.; Broussely, M.; Perton, F.; Biensan, P.; Willmann, P. *J. Phys. Chem. Solids* **1996**, *57*, 1057.
(4) Kanno, R.; Kubo, H.; Kawamoto, Y.; Kamiyama, T.; Izumi, F.; Takeda, Y.; Takano, M. *J. Solid State Chem.* **1994**, *110*, 216.
(5) Ohzuku, T.; Ueda, A.; Kouguchi, M. *J. Electrochem. Soc.* **1995**, *142*, 4033.
(6) Zhong, Q. M.; Vonsacken, U. *J. Power Sources* **1995**, *54*, 221.
(7) Guilmard, M.; Rougier, A.; Grune, A.; Croguennec, L.; Delmas, C. *J. Power Sources* **2003**, *115*, 305.
(8) Makimura, Y.; Ohzuku, T. *J. Power Sources* **2003**, *119*, 156.
(9) Kang, S. H.; Amine, K. *J. Power Sources* **2003**, *119*, 150.
(10) Jiang, J.; Dahn, J. R. *Electrochim. Acta* **2005**, *50*, 4778.
(11) Jiang, J.; Eberman, K. W.; Krause, L. J.; Dahn, J. R. *J. Electrochem. Soc.* **2005**, *152*, A566.
(12) Myung, S. T.; Komaba, S.; Kurihara, K.; Hosoya, K.; Kumagai, N.; Sun, Y. K.; Nakai, I.; Yonemura, M.; Kamiyama, T. *Chem. Mater.* **2006**, *18*, 1658.
(13) Ohzuku, T.; Makimura, Y. *Chem. Lett.* **2001**, *30*, 744.

10.1021/cm800314d CCC: $40.75
Published on Web 07/03/2008

The electronic structure of Ni ions in $LiNi_{0.5}Mn_{0.5}O_2$ is unique: $Ni^{3+}(t_{2g}^6e_g^1)$ in $LiNiO_2$ is changed to $Ni^{2+}(t_{2g}^6e_g^2)$ upon substitution of $Mn^{4+}(t_{2g}^3e_g^0)$. Lithium removal from $LiNi^{2+}_{0.5}Mn^{4+}_{0.5}O_2$ is accompanied by oxidation of Ni^{2+} to Ni^{4+} via Ni^{3+} while Mn^{4+} remains electrochemically inactive.[18–21] DSC and accelerating rate calorimetry (ARC) measurements in the presence of electrolyte have been used primarily to study the thermal stability of $Li_xNi_{0.5}Mn_{0.5}O_2$ electrodes. DSC data reported by Makimura and Ohzuku[8] have shown that fully charged $Li_{0.11}Ni_{0.5}Mn_{0.5}O_2$ (without carbon or binder) containing a small amount of $LiPF_6$/EC:DMC electrolyte solution has similar onset and peak temperatures of ~200 °C but with much reduced heat generation relative to NiO_2. In addition, ARC results[10,11] have suggested that $Li_xNi_{0.5}Mn_{0.5}O_2$ electrodes charged to 4.2 or 4.4 V in a $LiPF_6$/EC:DEC electrolyte have onset temperatures of ~190 °C and broad, exothermic peak temperatures of 240−280 °C. However, other DSC studies have revealed higher onset and peak temperatures of ~270 to ~280 °C for exothermic reactions of $Li_xNi_{0.5}Mn_{0.5}O_2$ electrodes charged to 4.3 V[9] (x is not reported) and 4.6 V[12] ($x = 0.25$) in the presence of a $LiPF_6$/EC:DEC electrolyte. Although these thermal measurements are sensitive to probe the thermal behavior of electrode materials under abuse conditions, the onset and peak temperatures of exothermic reactions can be affected strongly by the type[22,23] and amount[11] of electrolyte solution, particle size, and particle surface chemistry (the electrolyte−particle interface) of active materials[24] and heating rates.[25] Therefore, it is difficult to probe the mechanism by which thermal decomposition (typically endothermic reactions associated with substantial oxygen loss from bulk) of the layered $Li_xNi_{0.5}Mn_{0.5}O_2$ structure occurs and to compare its thermal stability relative to Li_xNiO_2 and its stabilized derivatives such as $Li_xNi_{0.7}Co_{0.15}Al_{0.15}O_2$.[26,27]

Ex situ and in situ X-ray diffraction measurements allow the study of structural transitions of electrode materials as a function of temperature, which is essential to understand the thermal behavior of electrode materials. Previous studies[25–30] of electrodes in the absence of electrolyte have shown that the layered structure of Li_xNiO_2 is shown to first transform to a pseudospinel structure upon heating to relatively low temperatures (~150 °C for $x = 0.3$) and then convert to a rocksalt-type phase with significant oxygen loss[26,27,30] at high temperatures (~270 °C for $x = 0.3$). In general, the stability of the layered structure relative to the pseudospinel structure decreases and the extent of oxygen loss increases with decreasing Li content in the Li_xNiO_2.[26,27,29,30] The improved thermal stability of $Li_xAl_{0.16}Ni_{0.89}O_2$ ($x = 0.3$ and 0.5) relative to Li_xNiO_2 has been attributed to the movement of Al^{3+} ions into tetrahedral sites from octahedral sites in the metal slabs, which impedes further cation migration necessary for the formation of pseudospinel and rocksalt phases and shifts the phase transitions to higher temperatures.[26,27] Manganese substitution in $Li_xMn_{0.11}Ni_{0.95}O_2$ appears to have a similar effect in stabilizing the pseudospinel structure to aluminum addition, which leads to improved thermal behavior.[27] A recent X-ray diffraction study[31] has reported that an $Li_{0.2}Ni_{0.5}Mn_{0.5}O_2$ electrode in the presence of electrolyte converts to the rocksalt phase upon oxygen loss at 340 °C, and this decomposition temperature is shown to be higher than those of $Li_{0.33}NiO_2$ (210 °C) and $Li_{0.27}Ni_{0.8}Co_{0.15}Al_{0.05}O_2$ (245 °C). However, discrepancy exists in the decomposition temperature of $Li_{0.2}Ni_{0.5}Mn_{0.5}O_2$ between X-ray powder diffraction[31] and DSC (the temperature of heat release at ~275 °C)[12] findings, both of which have been measured with electrolyte. To compare the intrinsic thermal stability of $Li_xNi_{0.5}Mn_{0.5}O_2$ electrodes with that of Li_xNiO_2-related electrodes, which have been well studied upon heating without electrolyte,[25–30] we examine the thermal decomposition of $Li_xNi_{0.5}Mn_{0.5}O_2$ electrodes without electrolyte by in situ X-ray powder diffraction and thermogravimetric analysis (TGA). We report X-ray diffraction data of pristine $LiNi_{0.5}Mn_{0.5}O_2$ powder and $Li_xNi_{0.5}Mn_{0.5}O_2$ electrodes cycled to 4.5 V in the temperature range from 25 to 600 °C collected in situ in argon by using synchrotron radiation with a Debye−Scherrer camera. Phase transitions and changes in the cation distribution of the layered structure (space group $R\bar{3}m$) in the charged ($x = 0.2$) and discharged ($x = 0.9$) electrodes will be reported. The mechanism of thermal decomposition of $Li_xNi_{0.5}Mn_{0.5}O_2$ electrodes will be proposed and discussed with respect to their improved thermal stability and excellent stability upon cycling to ~5 V.

Experimental Section

A pristine $LiNi_{0.5}Mn_{0.5}O_2$ sample was prepared from heat-treating lithium hydroxide and coprecipitated nickel manganese mixed-hydroxide at 1000 °C for 12 h in air and quenching to room temperature (RT). The detailed preparation procedure can be found in earlier studies.[14,16] This sample was shown to have ~0.10 Ni and Li interlayer mixing per formula unit in the rhombohedral layered structure[17] and to exhibit superlattice reflections that could

(14) Lu, Z. H.; MacNeil, D. D.; Dahn, J. R. *Electrochem. Solid State Lett.* **2001**, *4*, A191.
(15) Lu, Z. H.; Beaulieu, L. Y.; Donaberger, R. A.; Thomas, C. L.; Dahn, J. R. *J. Electrochem. Soc.* **2002**, *149*, A778.
(16) Breger, J.; Meng, Y. S.; Hinuma, Y.; Kumar, S.; Kang, K.; Shao-Horn, Y.; Ceder, G.; Grey, C. P. *Chem. Mater.* **2006**, *18*, 4768.
(17) Yabuuchi, N.; Kumar, S.; Li, H. H.; Kim, Y. T.; Shao-Horn, Y. *J. Electrochem. Soc.* **2007**, *154*, A566.
(18) Yoon, W. S.; Grey, C. P.; Balasubramanian, M.; Yang, X. Q.; McBreen, J. *Chem. Mater.* **2003**, *15*, 3161.
(19) Johnson, C. S.; Kim, J. S.; Kropf, A. J.; Kahaian, A. J.; Vaughey, J. T.; Fransson, L. M. L.; Edstrom, K.; Thackeray, M. M. *Chem. Mater.* **2003**, *15*, 2313.
(20) Koyama, Y.; Makimura, Y.; Tanaka, I.; Adachi, H.; Ohzuku, T. *J. Electrochem. Soc.* **2004**, *151*, A1499.
(21) Reed, J.; Ceder, G. *Electrochem. Solid State Lett.* **2002**, *5*, A145.
(22) MacNeil, D. D.; Dahn, J. R. *J. Electrochem. Soc.* **2003**, *150*, A21.
(23) Belharouak, I.; Lu, W. Q.; Vissers, D.; Amine, K. *Electrochem. Commun.* **2006**, *8*, 329.
(24) Cho, J.; Kim, Y. W.; Kim, B.; Lee, J. G.; Park, B. *Angew. Chem., Int. Ed.* **2003**, *42*, 1618.
(25) Dahn, J. R.; Fuller, E. W.; Obrovac, M.; Vonsacken, U. *Solid State Ionics* **1994**, *69*, 265.
(26) Guilmard, M.; Croguennec, L.; Denux, D.; Delmas, C. *Chem. Mater.* **2003**, *15*, 4476.
(27) Guilmard, M.; Croguennec, L.; Delmas, C. *Chem. Mater.* **2003**, *15*, 4484.
(28) Thomas, M.; David, W. I. F.; Goodenough, J. B.; Groves, P. *Mater. Res. Bull.* **1985**, *20*, 1137.
(29) Lee, K. K.; Yoon, W. S.; Kim, K. B.; Lee, K. Y.; Hong, S. T. *J. Power Sources* **2001**, *321*, 97–8.
(30) Arai, H.; Okada, S.; Sakurai, Y.; Yamaki, J. *Solid State Ionics* **1998**, *109*, 295.
(31) Yoon, W. S.; Chung, K. Y.; Balasubramanian, M.; Hanson, J.; McBreen, J.; Yang, X. Q. *J. Power Sources* **2006**, *163*, 219.

be indexed consistently to the $\sqrt{3}a_{hex.} \times \sqrt{3}a_{hex.} \times c_{hex.}$ superstructure with space group $P3_112$.[32–34] $Li_xNi_{0.5}Mn_{0.5}O_2$ samples were prepared by electrochemical cycling to 4.5 V under a current density of C/50 (5.6 mA/g) in 2016 coin cells. A reversible capacity of ~185 (mA h)/g was obtainable at C/50 in the voltage range of 2.5 and 4.5 V vs Li at RT, where detailed cell assembly and properties of $Li_xNi_{0.5}Mn_{0.5}O_2$ electrodes can be found in our previous papers.[17,34] The lithium contents in the charged and discharged electrodes were estimated from the charge passed in the lithium cells, which gave rise to $Li_{0.2}Ni_{0.5}Mn_{0.5}O_2$ and $Li_{0.9}Ni_{0.5}Mn_{0.5}O_2$, respectively.

Synchrotron radiation of BL02B2 at SPring-8 (Sayo-gun, Hyogo, Japan), equipped with a large Debye−Scherrer camera,[35] was used to collect X-ray diffraction data of pristine $LiNi_{0.5}Mn_{0.5}O_2$ powder and $Li_xNi_{0.5}Mn_{0.5}O_2$ electrodes as a function of temperature. The incident beam was adjusted to a wavelength of 0.5 Å by a Si(111) monochromator to minimize the absorption by the samples. The wavelength was calibrated to be 0.501 Å by using CeO_2 standard. The data were collected in the range of 0 to 75° in 2θ. A few milligrams of each sample in the powder form was placed in an Ar-filled quartz capillary (0.5 mm diameter and approximately 2 cm height) during the measurement. Argon gas having a purity of 99.999% was filled in the capillary. The temperature was increased at a regular interval of 50 °C from 100 °C and above, with the exception of an interval of 25 °C from 200 to 300 °C. The temperature ramp-up for each step was completed in 1 min by blowing hot air directly to the sample capillary. After reaching each target temperature, the sample was held during 25 min before measurement, and then X-ray diffraction data were recorded on the imaging plate for 5 min.

The changes in the lattice constants of the rhombohedral $Li_xNi_{0.5}Mn_{0.5}O_2$ structure ($R\bar{3}m$) in a hexagonal setting as a function of temperature were calculated by using X'Pert HighScore Plus (PANalytical). The lattice parameters of the rhombohedral structure determined from X'Pert HighScore Plus (PANalytical) software are in excellent agreement with those from the Rietveld refinement using FullProf. Rietveld refinement analysis including cation distributions in the rhombohedral structure and isotropic atomic displacement parameters was performed using FullProf[36] in the range of 10−45° in 2θ (d-spacing of 2.87−0.65 Å), which included more than 50 reflections. To avoid contributions originated from carbon and binder in the electrodes, the $(003)_{hex.}$ Bragg peak was excluded in the refinements. Since an isotropic atomic displacement parameter and occupancy of each site are highly correlated, the following restrictions on the refined parameters were imposed: (1) for the pristine $LiNi_{0.5}Mn_{0.5}O_2$ at RT, isotropic atomic displacement parameters were chosen and fixed, and only occupancies of nickel and lithium ions on the 3a and 3b sites were refined; (2) for the pristine $LiNi_{0.5}Mn_{0.5}O_2$ in the temperature range between 100 − 600 °C, occupancies were fixed based on the refined values obtained at RT, and isotropic displacement parameters on the 3a and 6c sites were refined as a function of temperature; and (3) for the charged and discharged $Li_xNi_{0.5}Mn_{0.5}O_2$ electrodes in the temperature range between 25 and 600 °C, isotropic atomic displacement parameters were chosen based on the refined values obtained from the pristine sample at each temperature, and the occupancies of nickel and lithium ions on the 3a and 3b sites were refined. The isotropic displacement parameters of octahedral 3a (primarily transition metal ions) and octahedral 6c (oxygen) sites of the pristine $LiNi_{0.5}Mn_{0.5}O_2$ sample were selected to be 0.3 and 0.7 at RT, respectively, based on reported values of $Li_xNi_{0.5}Mn_{0.5}O_2$ samples from synchrotron X-ray powder diffraction refinements.[37–39] It is noted that isotropic displacement parameters found for Me on the 3a sites (0.75) and for O on the 6c sites (1.5) at 600 °C are in good agreement with those reported previously for metal oxides[40] at high temperatures. The isotropic displacement parameter of the octahedral 3b sites (primarily lithium ions) in the charged electrode was chosen to be higher (1.2)[41] for having a larger fraction of vacancies than those of the pristine powder (1.0) and the discharged electrode (1.0) at RT. In addition, this parameter was set to linearly increase to 2.0 at 600 °C for the rhombohedral structure in the pristine sample as a higher value than that (1.5) of oxygen at 600 °C that is expected based on the difference in the atomic mass. As some nickel and lithium ions were found previously in the tetrahedral 6c (nickel and lithium ions) sites of charged and discharged electrodes at RT,[16,17,34] the occupancy of these tetrahedral sites in the layered structure were refined as a function of temperature in this study. The isotropic displacement parameters of the 6c sites were selected to be 0.6, which is larger than that of transition metal 3a sites and smaller than that of the oxygen 6c sites.

Thermogravimetric measurements of pristine $LiNi_{0.5}Mn_{0.5}O_2$ powder, and electrodes of pristine $LiNi_{0.5}Mn_{0.5}O_2$, charged $Li_{0.2}Ni_{0.5}Mn_{0.5}O_2$, and discharged $Li_{0.9}Ni_{0.5}Mn_{0.5}O_2$ by using TG/DTA-320 (Seiko Instruments) in the temperature range of 25−600 °C, from which weight loss was obtained as a function of temperature. A few milligrams of samples was loaded on an aluminum pan and was heated at a rate of 5.0 °C/min under a flow of nitrogen gas (150 mL/min). The purity of nitrogen gas used was 99.997%.

Results

Thermal Expansion of Pristine $LiNi_{0.5}Mn_{0.5}O_2$ (25−600 °C). Figure 1 shows powder X-ray diffraction patterns of pristine $LiNi_{0.5}Mn_{0.5}O_2$ in the temperature range between 25 and 600 °C, where no phase transition was noted. No change in the cation distribution of rhombohedral $LiNi_{0.5}Mn_{0.5}O_2$ ($R\bar{3}m$) upon heating was detected from the Rietveld refinement analyses. This is in contrast to the heating of an ion-exchanged "$LiNi_{0.5}Mn_{0.5}O_2$" sample[42] (having ~4% interlayer mixing of Li and Ni per formula unit) prepared from $NaNi_{0.5}Mn_{0.5}O_2$, which was shown to exhibit a distinct phase transition at ~600 °C, and a considerable amount of Ni (0.07 per formula unit) was found to migrate to the Li layer upon heating to 800 °C. All the diffraction peaks in Figure 1 were found to shift to lower angles as the temperature was increased. The lattice parameters of $a_{hex.}$ and $c_{hex.}$ and the $c_{hex.}/a_{hex.}$ ratio of the rhombohedral structure in the hexagonal unit cell setting were shown to increase

(32) Meng, Y. S.; Ceder, G.; Grey, C. P.; Yoon, W. S.; Shao-Horn, Y. *Electrochem. Solid State Lett.* **2004**, *7*, A155.
(33) Meng, Y. S.; Ceder, G.; Grey, C. P.; Yoon, W. S.; Jiang, M.; Breger, J.; Shao-Horn, Y. *Chem. Mater.* **2005**, *17*, 2386.
(34) Li, H. H.; Yabuuchi, N.; Meng, Y. S.; Kumar, S.; Breger, J.; Grey, C. P.; Shao-Horn, Y. *Chem. Mater.* **2007**, *19*, 2551.
(35) Nishibori, E.; Takata, M.; Kato, K.; Sakata, M.; Kubota, Y.; Aoyagi, S.; Kuroiwa, Y.; Yamakata, M.; Ikeda, N. *Nucl. Instrum. Methods Phys. Res., Sect. A* **2001**, *467*, 1045.
(36) Rodriguezcarvajal, J. *Physica B* **1993**, *192*, 55.
(37) Arachi, Y.; Kobayashi, H.; Emura, S.; Nakata, Y.; Tanaka, M.; Asai, T.; Sakaebe, H.; Tatsumi, K.; Kageyama, H. *Solid State Ionics* **2005**, *176*, 895.
(38) Kobayashi, H.; Arachi, Y.; Kageyama, H.; Tatsumi, K. *J. Mater. Chem.* **2004**, *14*, 40.
(39) Kobayashi, H.; Sakaebe, H.; Kageyama, H.; Tatsumi, K.; Arachi, Y.; Kamiyama, T. *J. Mater. Chem.* **2003**, *13*, 590.
(40) Rodriquez-Carvajal, J.; Hennion, M.; Moussa, F.; Pinsard, L.; Revcolevschi, A. *Physica B* **1997**, *234*, 848.
(41) Carlier, D.; Croguennec, L.; Ceder, G.; Menetrier, M.; Shao-Horn, Y.; Delmas, C. *Inorg. Chem.* **2004**, *43*, 914.
(42) Hinuma, Y.; Meng, Y. S.; Kang, K. S.; Ceder, G. *Chem. Mater.* **2007**, *19*, 1790.

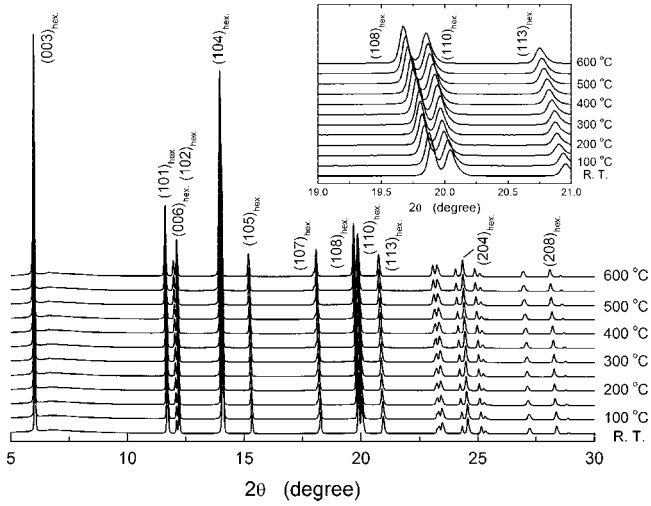

Figure 1. X-ray diffraction patterns of the pristine $LiNi_{0.5}Mn_{0.5}O_2$ sample at elevated temperatures in the ranges of 25−600 °C. The inset shows highlighted $(108)_{hex.}$ and $(110)_{hex.}$ Bragg peaks. A clear peak separation of the $(108)_{hex.}$ and $(110)_{hex.}$ reflections is observed as the increase in the temperature, indicating nonisotropic thermal expansion on the pristine $LiNi_{0.5}Mn_{0.5}O_2$.

linearly with increasing temperature, as shown in Figure 2a,b, respectively. The linear thermal expansion coefficients of the $a_{hex.}$ and $c_{hex.}$ axes are defined by using the following equations:

$$\alpha(a_{hex.}) = \frac{1}{a_{hex.RT}} \frac{da_{hex.}}{dT} \quad (1)$$

$$\alpha(c_{hex.}) = \frac{1}{c_{hex.RT}} \frac{dc_{hex.}}{dT} \quad (2)$$

where $a_{hex.RT}$ and $c_{hex.RT}$ are the lattice parameters at RT. It is interesting to note that the linear thermal expansion coefficient of the $c_{hex.}$ axis, $\alpha(c_{hex.}) = 2.21 \times 10^{-5}$ °C^{-1} (25−600 °C), is considerably larger than that of the $a_{hex.}$ axis, $\alpha(a_{hex.}) = 1.68 \times 10^{-5}$ °C^{-1} (25−600 °C), which leads to greater $c_{hex.}/a_{hex.}$ ratios at higher temperatures. In addition, the oxygen positional parameter (z) of the rhombohedral structure was found to increase very slightly from 0.2580(3) at 25 °C to 0.2585(3) at 600 °C. Therefore, the LiO_2 slab space ($\alpha(LiO_2) = 3.4 \times 10^{-5}$ °C^{-1}) expanded more than the MeO_2 slab space ($\alpha(MeO_2) = 1.1 \times 10^{-5}$ °C^{-1}) upon heating, as shown in Figure 2c. This anisotropy in thermal expansion can be explained by the fact that weak Li−O bonds expand more than strong Me−O (Ni^{2+}−O and Mn^{4+}−O) bonds with increasing temperature (Supporting Information Figure S1). Moreover, the volumetric thermal expansion coefficient of $LiNi_{0.5}Mn_{0.5}O_2$, β, was calculated to be 5.64×10^{-5} °C^{-1} between 25 and 600 °C (Supporting Information Figure S2). It is interesting to note that the volumetric thermal expansion coefficient of $LiNi_{0.5}Mn_{0.5}O_2$ is similar to that of NiO ($\beta = 5.4 \times 10^{-5}$ °C^{-1})[43] and is considerably larger than those of MnO ($\beta = 3.4-4.7 \times 10^{-5}$ °C^{-1})[44] and $Li_{0.25}Ni_{0.75}O_2$ ($\beta = 4.2 \times 10^{-5}$ °C^{-1}).[43]

Given the occupancies of the transition metal (3a), lithium (3b), and oxygen (6c) sites equal to unity, Rietveld refinement

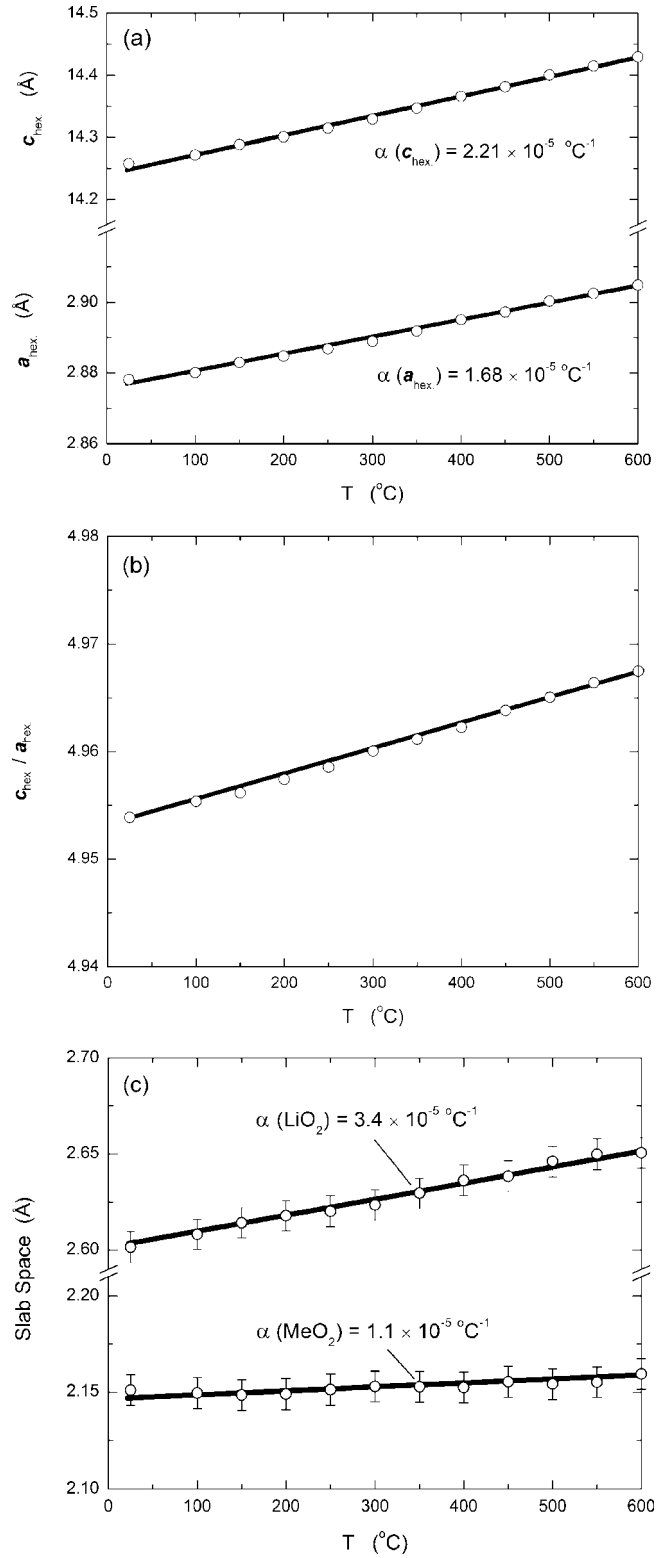

Figure 2. Change in crystallographic parameters on the pristine $LiNi_{0.5}Mn_{0.5}O_2$ sample as a function of the temperature in the range of 25 to 600 °C: (a) the lattice parameters, (b) $c_{hex.}/a_{hex.}$ ratio, and (c) the change in the MeO_2 and LiO_2 slab space.

of synchrotron X-ray diffraction data allows the refinement of the isotropic parameters of these sites as a function of temperature. Figure 3 shows the change in the isotropic displacement parameters for each site. The isotropic parameters of transition metal 3a and oxygen 6c sites were found to increase almost linearly from 0.30 Å^2 and 0.70 Å^2 at 25 °C

(43) Toussaint, C. *J. Appl. Crystallogr.* **1971**, *4*, 293.
(44) Suzuki, I. O.; Shinichi; Seya, K. *J. Phys. Earth* **1979**, *27*, 63.

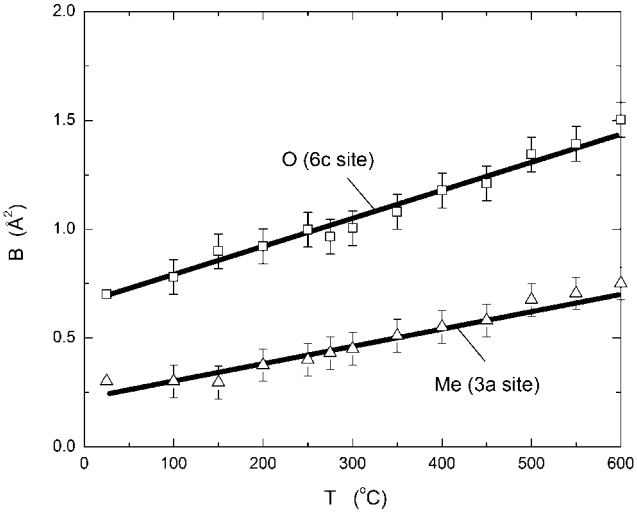

Figure 3. Isotropic displacement parameters (*B*) refined by Rietveld analysis of $LiNi_{0.5}Mn_{0.5}O_2$ data as a function of the temperature in the range of 25−600 °C. For 3b site (predominantly lithium ion), a linear increase in the values from 1.0 at 25 °C to 2.0 at 600 °C (without refining) is assumed as the refinement of lithium ions using synchrotron X-ray diffraction data is difficult. The occupancies were fixed based on the values refined at 25 °C in the entire temperature range.

to 0.75 Å^2 and 1.50 Å^2 at 600 °C, respectively. As expected, the increase in the isotropic atomic displacement parameter of oxygen 6c sites upon heating is much greater than that of transition metal 3a sites. The slope of the increment in the isotropic displacement parameters is calculated to be 1.3×10^{-3} Å^2/°C for oxygen and 0.8×10^{-3} Å^2/°C for metal ions. The information is used to estimate the change in the isotropic parameters of lithium, oxygen, and transition metal sites in the rhombohedral structure of the charged and discharged $Li_xNi_{0.5}Mn_{0.5}O_2$ electrodes at elevated temperatures, which is necessary for the Rietveld refinements of cation distributions as a function of temperature.

Structural Degradation of Cycled $Li_xNi_{0.5}Mn_{0.5}O_2$ (25−600 °C). In situ X-ray diffraction patterns of charged $Li_{0.2}Ni_{0.5}Mn_{0.5}O_2$ and discharged $Li_{0.9}Ni_{0.5}Mn_{0.5}O_2$ samples in the temperature range from 25 to 600 °C are shown in Figure 4a,c, respectively. At 275 °C and lower, only the rhombohedral structure ($R\bar{3}m$) was found. Upon heating to 300 °C and higher, two phase transitions were noted in the charged and discharged $Li_xNi_{0.5}Mn_{0.5}O_2$ electrodes: (i) 300−350 °C, a spinel-type M_3O_4 (M = Li and Me) structure ($Fd\bar{3}m$) became evident as shown by the appearance of the $(220)_{spinel}$ Bragg reflection in Figure 4a,c, which is characteristic of cation ordering on tetrahedral 8a sites; (ii) 450−500 °C, a rocksalt-type MO phase ($Fm\bar{3}m$) was formed. The temperatures of these two transitions were slightly higher in the discharged electrode relative to those of the charged sample. In addition to these two phase changes, a third phase transition was noted for the discharged electrode at 600 °C (but not in the charged sample), where a new, crystalline rhombohedral phase (relatively sharp peaks) and nickel metal were detected in the discharged sample. As the X-ray diffraction peaks of the spinel-type and rocksalt-type structures were found fairly broad (Figure 4), it is believed that these structures do not have cation arrangements or the stoichiometry of ideal spinel and rocksalt structures. In the following sections, we show in detail how the cation distribution of the rhombohedral structure in the charged and discharged samples changes as a function of temperature up to 275 °C and how the unit cell dimensions of rhombohedral, spinel-type and rocksalt-type structures change as a function of temperature up to 600 °C.

Changes in the cation distribution of the rhombohedral $R\bar{3}m$ structure (RT to 275 °C). The intensity ratio of the $(003)_{hex.}$ and $(104)_{hex.}$ reflections of the rhombohedral structure ($R\bar{3}m$) in $Li_{0.2}Ni_{0.5}Mn_{0.5}O_2$ was noted to considerably decrease with increasing temperature in Figure 4b while such a change was not noted in $Li_{0.9}Ni_{0.5}Mn_{0.5}O_2$ in Figure 4d. Reduction in the intensity ratio of the $(003)_{hex.}$ and $(104)_{hex.}$ reflections can result from changes in the cation distribution, in particular, migration from transition metal ions to the Li layer. This hypothesis is confirmed by the Rietveld refinement results. The crystallographic parameters, site occupancies of the 3a, 3b, and 6c sites of the rhombohedral $Li_{0.2}Ni_{0.5}Mn_{0.5}O_2$ structure, and corresponding refinement error values (R_{wp} and R_B) are compared with those of $Li_{0.9}Ni_{0.5}Mn_{0.5}O_2$ at select temperatures, as shown in Table 1. The calculated and observed spectra and their differential plots of $Li_{0.2}Ni_{0.5}Mn_{0.5}O_2$ at 200 and 275 °C and $Li_{0.9}Ni_{0.5}Mn_{0.5}O_2$ at 275 °C can be found in Supporting Information Figure S3, which were used to generate the refinement results in Table 1.

At 25 °C, the charged $Li_{0.2}Ni_{0.5}Mn_{0.5}O_2$ electrode has ∼0.03 nickel ions in the octahedral 3b sites of the Li layer and ∼0.03 nickel ions in the tetrahedral 6c sites per formula unit[17] while the discharged sample was found to have ∼0.06 and ∼0.02 nickel ions in the octahedral 3b and tetrahedral 6c sites per formula unit, respectively. These refinement results are consistent with previous findings,[16,17,34,37] which have shown that (1) octahedral Ni ions could migrate from the Li layer, thorough face-shared tetrahedral sites in the Li layer, into the transition metal layer upon charge; and (2) the process was in part reversible upon discharge.

Upon heating from 100 to 275 °C, the occupancy of the 3b sites in the Li layer (Li occupancy was fixed on the 3b sites) was found to considerably increase, and that of the 3a sites (transition metal layer) decreased in the charged sample. Approximately 0.15 interlayer mixing per formula unit was found in the charged sample at 275 °C, which suggests that a considerable amount of cations (∼0.09 cation per formula unit) has migrated from the Li layer to the transition metal layer upon heating. In contrast, no change in the cation distribution was detected with certainty in $Li_{0.9}Ni_{0.5}Mn_{0.5}O_2$ upon heating to 300 °C. As shown in Table 1, a relatively high R_{wp} value was obtained for the refinement of $Li_{0.2}Ni_{0.5}Mn_{0.5}O_2$ at 275 °C, which could be attributed to broadening of diffraction peaks and the onset of structural decomposition at this temperature (Supporting Information Figure S3b).

In the Rietveld refinements of data collected upon heating to 250 °C, only the reflections of the rhombohedral structure ($R\bar{3}m$) were considered, and oxygen occupancy in the rhombohedral structure was not refined because oxygen has a

(45) Adler, S. B. *J. Am. Ceram. Soc.* **2001**, *84*, 2117.

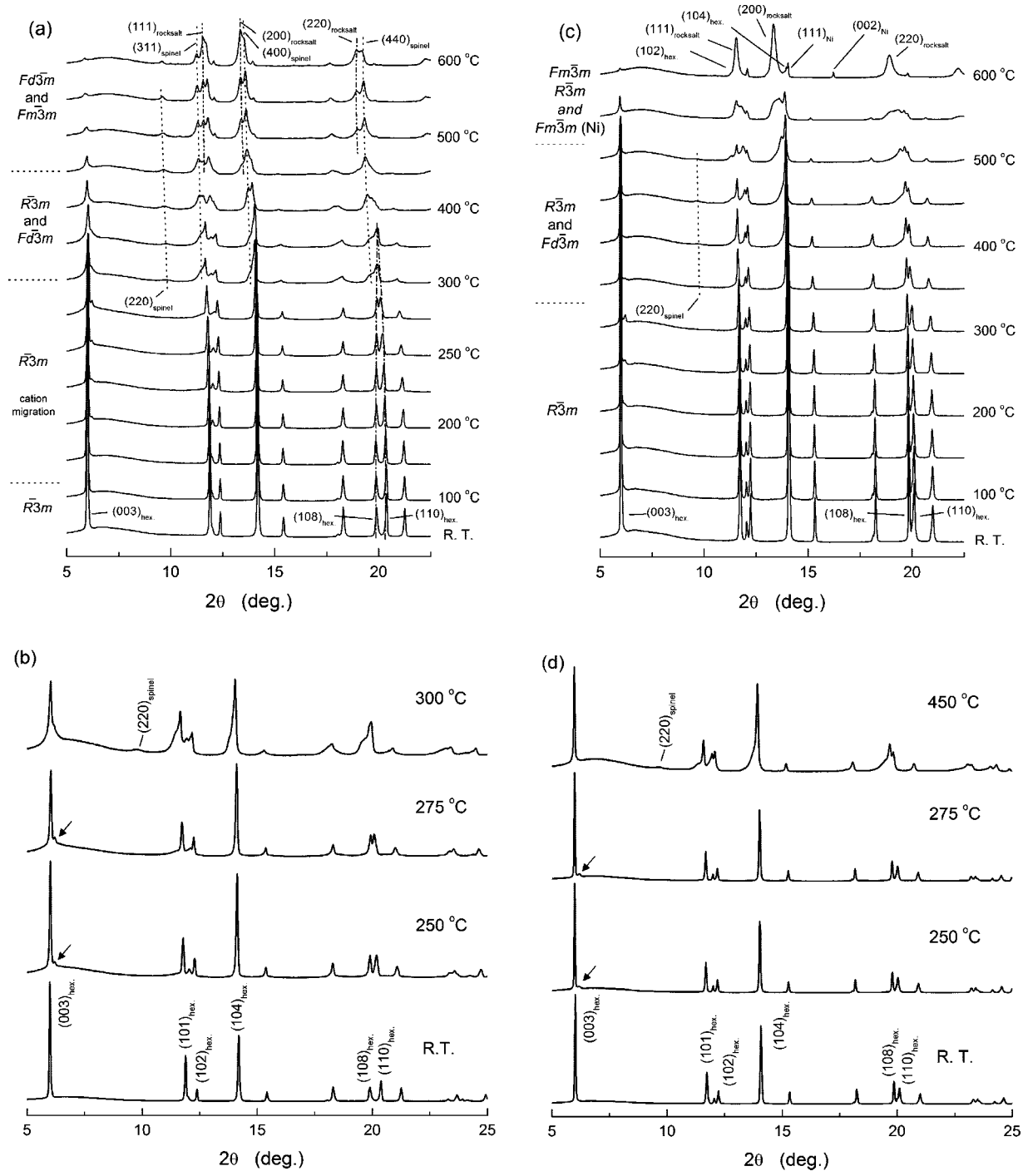

Figure 4. X-ray diffraction patterns of (a) 4.5 V charged $Li_{0.2}Ni_{0.5}Mn_{0.5}O_2$ and (c) discharged $Li_{0.9}Ni_{0.5}Mn_{0.5}O_2$ (after charging to 4.5 V) at elevated temperatures in the range of 25−600 °C. The highlighted X-ray diffraction patterns of (b) $Li_{0.2}Ni_{0.5}Mn_{0.5}O_2$ at 25, 250, 275, and 300 °C and (d) $Li_{0.9}Ni_{0.5}Mn_{0.5}O_2$ at 25, 250, 275, 300, and 450 °C. Arrows in the plots show unindexed peak with an interplanar spacing of 4.63 Å, close to the $(003)_{hex.}$ Bragg reflection of the parent rhombohedral phase.

considerably smaller atomic scattering factor for X-ray relative to transition metal ions. The formation of a considerable amount of oxygen vacancies in a given structure upon heating would typically lead to larger lattice expansion than pure thermal expansion (known as chemical expansion[45]). In this study, we postulate the extent of oxygen vacancy formation in the rhombohedral structure of charged and discharged electrodes from the expansion in the unit cell volume upon heating to 275 °C, which will be discussed in terms of detailed lattice parameter analysis and TGA data in later sections. Further neutron diffraction studies are needed to quantify to what extent oxygen vacancies are formed in the rhombohedral structure of $Li_xNi_{0.5}Mn_{0.5}O_2$ upon heating.

Changes in the Unit Cell Dimensions of Rhombohedral, Spinel-Type and Rocksalt-Type Structures. The unit cells of ideal spinel and rocksalt structures, which have cubic symmetry and a cubic close-packed oxygen array, are shown relative to the rhombohedral structure in Figure 5.[46] Lattice parameters of spinel and rocksalt phases can be related to

(46) Ohzuku, T.; Ariyoshi, M.; Makimura, Y.; Yabuuchi, N.; Sawai, K. *Electrochemistry* **2005**, *73*, 2.

Table 1. Crystallographic Parameters for $Li_{0.2}Ni_{0.5}Mn_{0.5}O_2$ Obtained by the Rietveld Analysis at 25, 100, 200, and 275 °C and $Li_{0.9}Ni_{0.5}Mn_{0.5}O_2$ at 25 and 275 °C[a]

composition		$Li_{0.2}Ni_{0.5}Mn_{0.5}O_2$ (4.5 V charged)				$Li_{0.9}Ni_{0.5}Mn_{0.5}O_2$ (4.5 V discharged)	
temperature (°C)		25	100	200	275	25	275
space group		$R\bar{3}m$	$R\bar{3}m$	$R\bar{3}m$	$R\bar{3}m$	$R\bar{3}m$	$R\bar{3}m$
lattice constants (Å)		$a_{hex.}$ = 2.8326(3)	$a_{hex.}$ = 2.8347(3)	$a_{hex.}$ = 2.8436(3)	$a_{hex.}$ = 2.8698(4)	$a_{hex.}$ = 2.8700(3)	$a_{hex.}$ = 2.8810(4)
		$c_{hex.}$ = 14.373(1)	$c_{hex.}$ = 14.389(1)	$c_{hex.}$ = 14.353(1)	$c_{hex.}$ = 14.257(1)	$c_{hex.}$ = 14.308(1)	$c_{hex.}$ = 14.366(1)
3a site	Ni (g)	0.439(4)	0.435(4)	0.395(8)	0.345(10)	0.419(3)	0.424(5)
	Mn (g)	0.5[b]	0.5[b]	0.5[b]	0.5[b]	0.5[b]	0.5[b]
	Li (g)	0[b]	0[b]	0[b]	0[b]	0.03[c,b]	0.03[c,b]
	B (Å^2)[d]	0.30[b]	0.31[b,e]	0.39[b,e]	0.45[b,e]	0.30[b]	0.45[b,e]
3b site	Li (g)	0.220[b]	0.220[b]	0.220[b]	0.220[b]	0.820[b]	0.820[b]
	Ni (g)	0.031(4)	0.039(4)	0.079(8)	0.135(10)	0.063(3)	0.056(5)
	B (Å^2)[d]	1.20[b]	1.33[b]	1.50[b]	1.63[b]	1.00[b]	1.43[b]
6c site	tetrahedral						
	Ni (g)	0.015(2)	0.013(2)	0.013(4)	0.010(5)	0.009(1)	0.009(2)
	B (Å^2)[d]	0.60[b]	0.68[b]	0.80[b]	0.88[b]	0.60[b]	0.88[b]
	octahedral						
	O (g)	1.00[b]	1.00[b]	1.00[b]	1.00[b]	1.00[b]	1.00[b]
	B (Å^2)[d]	0.70[b]	0.80[b,e]	0.92[b,e]	1.02[b,e]	0.70[b]	1.02[b,e]
positional parameter z for 6c site	Ni (tetrahedral)	0.133[f]	0.133[f]	0.132[f]	0.130[f]	0.130[f]	0.130[f]
	O (Octahedral)	0.2630(5)	0.2630(5)	0.2624(7)	0.2595(10)	0.2593(5)	0.2587(6)
unit cell volume (Å^3)		99.87	100.13	100.51	101.69	102.06	103.26
R_{wp} (%)		15.2	16.5	18.6	27.6	14.5	14.4
R_B (%)		6.2	8.5	8.6	15.1	4.1	6.0

[a] Rietveld analysis was carried out in the range of 10−40° in 2θ (λ = 0.501 Å), corresponding to the d-spacing of 2.87−0.73 Å. [b] Not refined. [c] Fixed with the assumption based on the observation of NMR study.[45] A small amount of lithium ions was observed after discharge. [d] Isotropic displacement parameter. [f] Fixed based on z for octahedral site. [e] Fixed based on the B values obtained for the pristine sample.

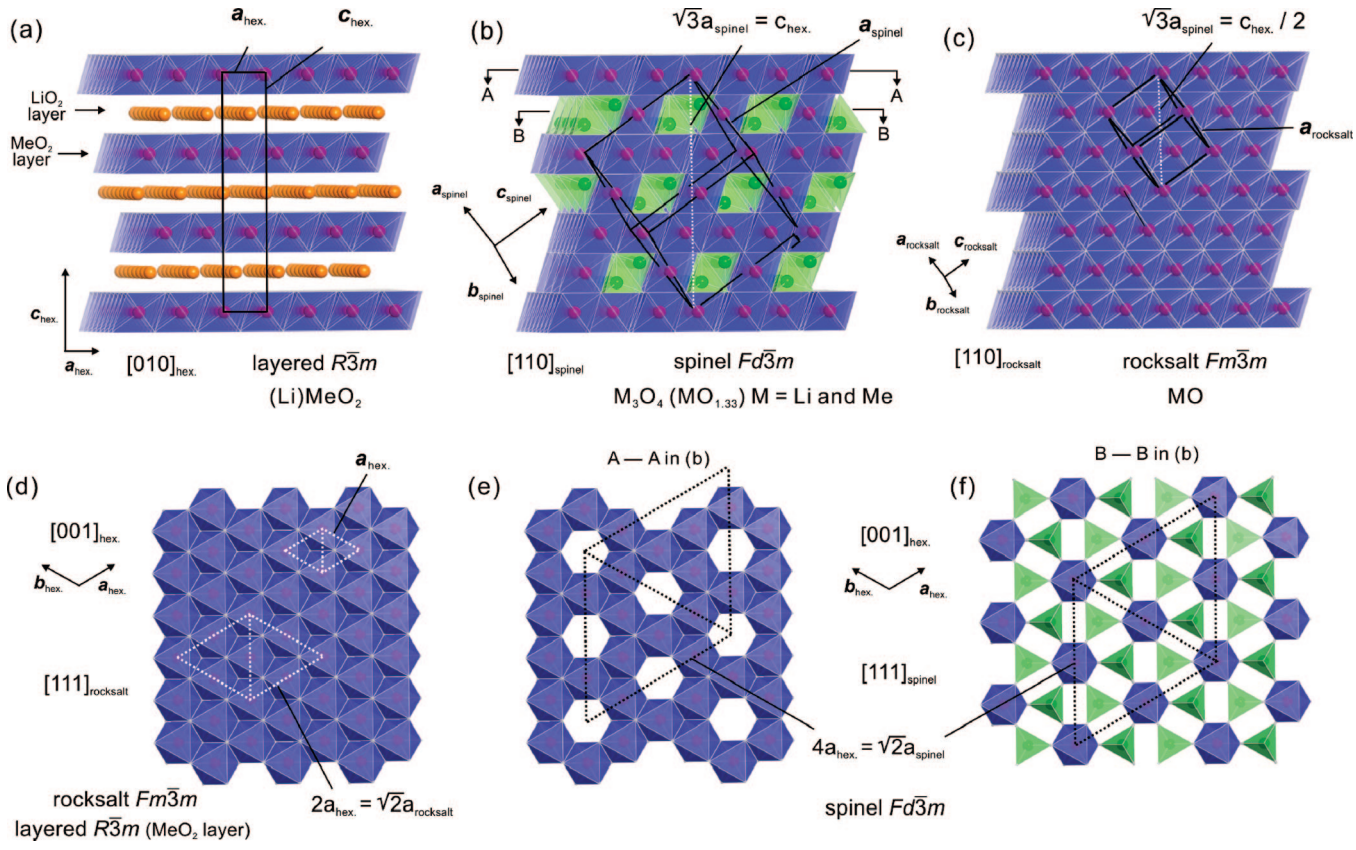

Figure 5. Schematic illustration of crystal structure of (a) an ideal layered material ($R\bar{3}m$), (b) a spinel structure ($Fd\bar{3}m$), and (c) a rocksalt structure as a layered formulation along the $[010]_{hex.}$ or $[110]_{cubic}$ direction. (d) A MeO_2 basal plane of the layered material projected along $[001]_{hex.}$ consisting of edge-shared MeO_6 octahedra and rocksalt structure with the same basal plane, which is perpendicular to $[111]_{cubic}$. The spinel structure has two kinds of basal planes as the layered formulation: (e) cations occupy octahedral sites only and 1/4 octahedral vacancies exists in the MeO_2 sheet and (f) cations occupy 1/4 octahedral site and 1/4 tetrahedral site in the MeO_2 sheet and the basal plane is built up by corner sharing MeO_6 octahedra and MeO_4 tetrahedra.

those of the rhombohedral structure in the hexagonal unit cell setting using the following relationships: $a_{spinel} = a_{hex.} \times 2\sqrt{2}$, $a_{spinel} = c_{hex.}/\sqrt{3}$ and $a_{rocksalt} = a_{hex.} \times \sqrt{2}$, and $a_{rocksalt} = c_{hex.}/2\sqrt{3}$. It should be noted that both spinel and rocksalt

structures have a $c_{hex.}/a_{hex.}$ ratio of 4.90 bound by the cubic symmetry unlike the rhombohedral structure. Using these relationships, the unit cell dimensions of spinel-type and rocksalt-type phases in the charged and discharged samples can be compared to those of the rhombohedral structure in the temperature range of 25 and 600 °C, as shown in Figures 6a−f. In these graphs, discontinuity in the lattice parameters as a function of temperature is indicative of a structural transition and the appearance of a new phase. Unit cell dimensions and thermal expansion coefficients of the rhombohedral, spinel-type and rocksalt-type phases observed at select temperatures are listed in Table 2.

Four important observations are made from Figure 6. First, the lattice parameters and $c_{hex.}/a_{hex.}$ ratio of the rhombohedral structure were found to considerably change in the charged sample as a function of temperature while those found in the discharged sample increased slightly from RT to 300 °C. In the case of $Li_{0.2}Ni_{0.5}Mn_{0.5}O_2$, it was found that $a_{hex.}$ continuously increased while $c_{hex.}$ decreased with rising temperature, which led to a sharp decrease in the $c_{hex.}/a_{hex.}$ ratio, as shown in Figure 6b. The change could be noted easily in the diffraction data as peak doublets of $(108)_{hex.}$ and $(110)_{hex.}$ and $(2016)_{hex.}$ and $(220)_{hex.}$, characteristic to the $R\bar{3}m$ structure, were found to gradually merge into single peaks upon heating to 300 °C, as shown in Figure 4. The $c_{hex.}/a_{hex.}$ ratio of rhombohedral $Li_xNi_{0.5}Mn_{0.5}O_2$ decreases to ∼4.90 as the temperature approaches 300 °C, which indicates that the cubic close-packed oxygen array of the rhombohedral structure approaches the cubic symmetry. At 275 °C, the rhombohedral $Li_{0.2}Ni_{0.5}Mn_{0.5}O_2$ structure was found to have unit cell dimensions of $a_{hex.} = 2.89$ Å and $c_{hex.} = 14.22$ Å and a $c_{hex.}/a_{hex.}$ ratio of 4.92, which is shown in Tables 1 and 2 and Figure 6b. The reduction in the $c_{hex.}/a_{hex.}$ ratio of the rhombohedral structure is consistent with the increasing transition metal occupancy in the Li layer as temperature was increased, which led to the decreased LiO_2 slab space and thus reduced lattice parameter $c_{hex.}$. In contrast, the $c_{hex.}/a_{hex.}$ ratio remains constant in the discharged sample up to ∼300 °C (Figure 6e), which is in good agreement with nearly constant cation distributions found from the Rietveld refinement (Table 1).

Second, the unit cell volume of the rhombohedral structure was found to increase linearly, and the increase in the unit cell volume of the charged and discharged samples as a function of temperature were calculated to be 4.06×10^{-5} $°C^{-1}$ (25−275 °C) and 4.63×10^{-5} $°C^{-1}$ (25−300 °C), respectively. These values are slightly smaller than the thermal expansion coefficients of pristine $LiNi_{0.5}Mn_{0.5}O_2$. The dotted line shown in Figure 6c,f corresponds to the thermal expansion in the unit volume of pristine $LiNi_{0.5}Mn_{0.5}O_2$ ($\beta = 5.64 \times 10^{-5}$ $°C^{-1}$). Therefore, the extent of oxygen vacancy formation (which typically leads to considerable lattice expansion[45]) in the charged and discharged $Li_xNi_{0.5}Mn_{0.5}O_2$ electrodes upon heating to 275 °C, is considered insignificant, which will be supported with TGA results shown in a later section. As the changes in the $a_{hex.}$ and $c_{hex.}$ of the $Li_{0.2}Ni_{0.5}Mn_{0.5}O_2$ rhombohedral structure from RT to 275 °C are affected not only by thermal expansion but also by cation migration from the transition metal layer to the Li layer, the values of $a_{hex.}$ and $c_{hex.}$ were found to first slightly increase and then decrease nonlinearly with increasing temperature (Figure 6a), respectively. This is in contrast to linear thermal expansion coefficients of $Li_{0.9}Ni_{0.5}Mn_{0.5}O_2$ unit cell dimensions in the temperature range from 25 to 300 °C (with no cation migration as shown in Figure 9), having $\alpha(a_{hex.}) = 1.39 \times 10^{-5}$ $°C^{-1}$ and $\alpha(c_{hex.}) = 2.21 \times 10^{-5}$ $°C^{-1}$, which are comparable to those of the pristine sample.

Third, the rhombohedral phase was preserved partly at temperatures greater than 300 °C, which was found to have $c_{hex.}/a_{hex.}$ ratios approaching 4.9. The rhombohedral and spinel-type phases were found to coexist upon heating of the charged electrode from 300 °C to 450 °C, and the spinel-type phase became the major phase at ∼400 °C (relative to the rhombohedral phase) for the charged electrode. This is in contrast to the observation that the rhombohedral phase remained as the major phase up to 500 °C for the discharged electrode. Although X-ray diffraction data in this study appear similar to those reported previously,[31] detailed analyses reveal findings different from the previous study,[31] which reports that the spinel-type phase is the dominant phase at ∼335 °C (Figure 3b of this previous study[31]) and the formation of rocksalt-type phase occurs at ∼340 °C. We here use two models to show X-ray diffraction evidence of rhombohedral-type and spinel-type phases at ∼300 °C in the charged electrode: (1) single-phase spinel-type model and (2) two-phase model that consists of both rhombohedral-type and spinel-type phases. When the single-phase model was employed, a clear deviation in the calculated and observed peak positions was confirmed, especially for the $(220)_{spinel}$ peak (Figure 7a inset), as shown in Figure 7a. When the two-phase model was applied, an excellent agreement between the calculated and the observed peak positions was obtained, as shown in Figure 7b. The spinel-type peaks are locating at lower angles of the rhombohedral-type reflections, which lead to apparent peak broadening and peak asymmetry at this temperature. Moreover, much greater increases in the unit cell volume as a function of temperature were noted for the rhombohedral-type phase ($R\bar{3}m$) in the charged (45×10^{-5} $°C^{-1}$) and discharged (14×10^{-5} $°C^{-1}$) samples relative to $LiNi_{0.5}Mn_{0.5}O_2$ at 300 °C and higher, as shown in Figure 6c,f, respectively. These values are significantly larger than volumetric thermal expansion coefficients of oxides, which are typically less than 10×10^{-5} $°C^{-1}$.[47] Therefore, it is postulated that the rhombohedral-type structure gradually loses oxygen upon heating at temperatures higher than ∼275 °C, which can reduce the valence of transition metal ions and increase the unit cell volume in addition to thermal expansion. The stability of the rhombohedral-type phase and its coexistence with the spinel-phase at 300 °C and higher can suggest lower oxygen loss relative to complete conversion to the spinel-type phase. It should be noted that the increase in the unit cell volume of the rhombohedral structure in $Li_{0.2}Ni_{0.5}Mn_{0.5}O_2$ as a function of temperature at temperatures greater than ∼275 °C is considerably greater than that found in $Li_{0.9}Ni_{0.5}Mn_{0.5}O_2$, which indicates greater oxygen loss from $Li_{0.2}Ni_{0.5}Mn_{0.5}O_2$.

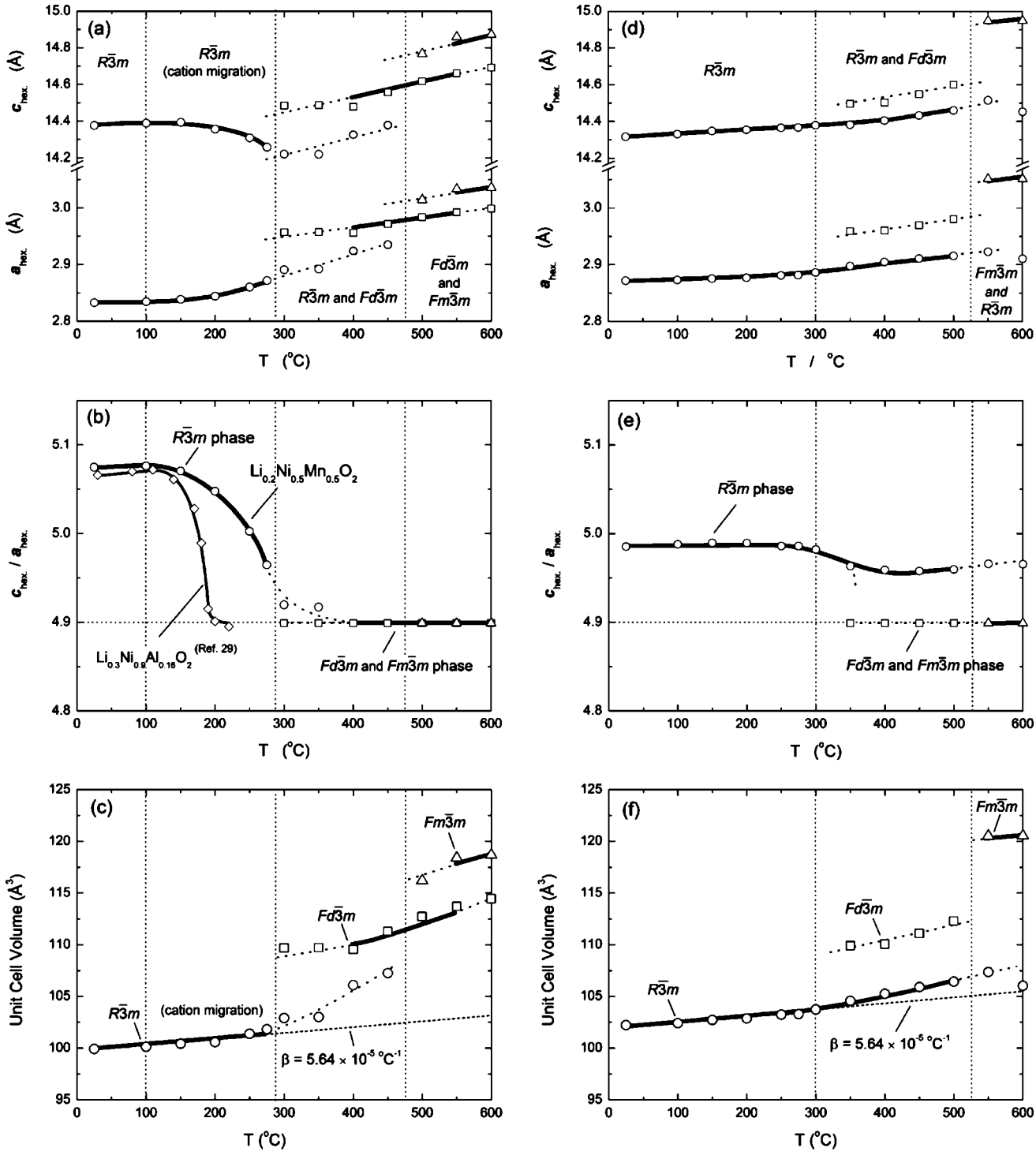

Figure 6. Change in the lattice parameters of (a) charged $Li_{0.2}Ni_{0.5}Mn_{0.5}O_2$ and (d) discharged $Li_{0.9}Ni_{0.5}Mn_{0.5}O_2$ in the range of 25−600 °C. The lattice parameters of spinel-type or rocksalt-type structure were converted to that of α-$NaFeO_2$-type in a hexagonal setting. The changes in the ratio of $c_{hex.}/a_{hex.}$ for (b) $Li_{0.2}Ni_{0.5}Mn_{0.5}O_2$ and (e) $Li_{0.9}Ni_{0.5}Mn_{0.5}O_2$ in the range of 25−600 °C are also shown. A cubic phase such as spinel and rocksalt structures has the ratio of $c_{hex.}/a_{hex.} = 4.9$. The change in the ratio $c_{hex.}/a_{hex.}$ for $Li_{0.3}Ni_{0.9}Al_{0.16}O_2$ is also plotted in (b) for comparison.[26] The unit cell volumes for (c) $Li_{0.2}Ni_{0.5}Mn_{0.5}O_2$ and (f) $Li_{0.9}Ni_{0.5}Mn_{0.5}O_2$ in the range of 25−600 °C were calculated from (a) and (d), respectively, with the slope observed for the pristine $LiNi_{0.5}Mn_{0.5}O_2$. Oxygen loss from the material probably leads to deviation from the slope and/or the noncontinuous change in the unit cell volume. The open circles, squares, and triangles correspond to the α-$NaFeO_2$ ($R\bar{3}m$), spinel ($Fd\bar{3}m$), and rocksalt ($Fm\bar{3}m$) structure, respectively.

Fourth, the unit cell volumes of the spinel-type and rocksalt-type phases found in the charged and discharged electrodes at temperatures greater than 300 °C in the charged and discharged samples are considerably larger than that of the rhombohedral phase, as shown in Figure 6c,f, respectively. For example, the spinel-type phase has a lattice parameter of $a_{spinel} = 8.36(1)$ Å ($a_{hex.} = 2.96$ Å and $c_{hex.} = 14.49$ Å) at 300 °C, which results in a unit cell volume ($V = 109.7$ Å^3) that is considerably larger than that of the rhombohedral phase ($a_{hex.} = 2.89$ Å and $c_{hex.} = 14.22$ Å; $V = 102.9$ Å^3). This large, discontinuous increase in the unit cell volume found in the cycled samples as a function of

Table 2. Crystallographic Parameters of Representative Phases Observed for the Charged and Discharged $Li_xNi_{0.5}Mn_{0.5}O_2$ Samples during Heating up to 600 °C[a]

sample	phase	temperature (°C)	space group	lattice parameters (Å)[b]	unit cell volume[b] (Å^3)	thermal expansion coeffecients (10^{-5} × °C^{-1})			remarks
						$\alpha(a_{hex.})$	$\alpha(c_{hex.})$	β (volume)	
pristine sample $LiNi_{0.5}Mn_{0.5}O_2$	rhombohedral	RT	$R\bar{3}m$	$a_{hex.} = 2.878$ $c_{hex.} = 14.258$	102.3	1.68	2.21	5.64	α and β were calculated in the range of 25−600 °C
		600	$R\bar{3}m$	$a_{hex.} = 2.905$ $c_{hex.} = 14.430$	105.4				
4.5 V charged state $Li_{0.2}Ni_{0.5}Mn_{0.5}O_2$	rhombohedral	RT	$R\bar{3}m$	$a_{hex.} = 2.833$ $c_{hex.} = 14.373$	99.9			4.06	β was calculated in the range of 25−275 °C
		275	$R\bar{3}m$	$a_{hex.} = 2.870$ $c_{hex.} = 14.257$	102.6				
	rhombohedral	400	$R\bar{3}m$	$a_{hex.} = 2.92$ $c_{hex.} = 14.33$	106.1				
	spinel-type	400	$Fd\bar{3}m$	$a_{spinel} = 8.36$ ($a_{hex.} = 2.96$ $c_{hex.} = 14.48$)	584.3(109.5)				
	rocksalt-type	600	$Fm\bar{3}m$	$a_{rocksalt} = 4.29$ ($a_{hex.} = 3.04$ $c_{hex.} = 14.87$)	79.1(119.0)				
4.5 V discharged state $Li_{0.9}Ni_{0.5}Mn_{0.5}O_2$	rhombohedral	RT	$R\bar{3}m$	$a_{hex.} = 2.870$ $c_{hex.} = 14.308$	102.1	1.39	1.55	4.63	α and β were calculated in the range of 25−300 °C
		300	$R\bar{3}m$	$a_{hex.} = 2.886$ $c_{hex.} = 14.379$	103.7				
	rhombohedral	450	$R\bar{3}m$	$a_{hex.} = 2.91$ $c_{hex.} = 14.43$	105.9				
	spinel-type	450	$Fd\bar{3}m$	$a_{spinel} = 8.40$ ($a_{hex.} = 2.97$ $c_{hex.} = 14.55$)	592.5(111.1)				
	rocksalt-type	600	$Fm\bar{3}m$	$a_{rocksalt} = 4.32$ ($a_{hex.} = 3.05$ $c_{hex.} = 14.95$)	80.4(120.4)				
	rhombohedral	600	$R\bar{3}m$	$a_{hex.} = 2.91$ $c_{hex.} = 14.45$	106.0				recrystallized phase nickel metal
	cubic-type	600	$Fm\bar{3}m$	$a_{cubic} = 3.55$	44.9				

[a] A maximum ESD of ±1% was found for the lattice parameters of various phases in this table. [b] The lattice paramters and unit cell volume in the brackets are the values assumed as a rhombohedral phase for comparison.

temperature supports that the spinel-type and rocksalt-type phases have reduced valence states of transition metal ions upon substantial oxygen loss from the rhombohedral phase. In addition, the increases in the unit cell volume for the spinel-type and rocksalt-type phase as a function of temperature is significantly larger than the slope obtained from the thermal expansion coefficients of pristine $LiNi_{0.5}Mn_{0.5}O_2$, NiO[43] and MnO,[44] as shown in Figure 6c,f. This suggests that the continuous oxygen loss from the spinel-type and rocksalt-type phase contributes to the unit volume augment with increasing temperature in addition to thermal expansion.

It should be mentioned that weak shoulder peaks in addition to fundamental peaks of the rhombohedral structure appeared at 275 °C in the charged sample (marked by arrows in Figure 4b) and at 300 °C in the discharged sample (marked by arrows in Figure 4d). These weak shoulder peaks were found to disappear upon the formation of the spinel-type structure in the charged and discharged samples upon heating to ~300 and ~350 °C, respectively. The physical origin of these weak shoulder peaks is not understood. The formation of structural defects (such as stacking faults) associated with a minute amount of oxygen loss may lead to the formation of an intermediate phase between the rhombohedral and spinel-type phases. Estimated from the intensity of the strongest weak shoulder peak having interplanar spacing of 4.63 Å at 275−300 °C, the percentage of this intermediate phase is no greater than 5% by volume in the charged and discharged samples.

TGA of $Li_xNi_{0.5}Mn_{0.5}O_2$. To further relate the changes in the crystal structures of $Li_xNi_{0.5}Mn_{0.5}O_2$ shown by X-ray diffraction studies to oxygen loss from the materials upon heating, weight loss percentages of pristine $LiNi_{0.5}Mn_{0.5}O_2$ and cycled electrodes were obtained from TGA under a continuous flow of nitrogen gas, as shown in Figure 8. The pristine $LiNi_{0.5}Mn_{0.5}O_2$ powder without carbon and binder shows no weight loss in the temperature range of 25 to 600 °C under nitrogen gas flowing. This result is consistent with the observation that no phase transition is detected, as shown in Figures 1 and 2, which supports the hypothesis that there is no oxygen loss upon heating $LiNi_{0.5}Mn_{0.5}O_2$ to 600 °C in the Rietveld analysis. Considerable weight loss (~1 wt %) was found to begin at ~260 °C for the charged electrode relative to the pristine $LiNi_{0.5}Mn_{0.5}O_2$ electrode. Release of some water molecules (1 wt % weight loss) associated with CO_2 desorption from charged $Li_{0.5}Ni_{1.02}O_2$ was reported in the temperature range from 150 and 250 °C previously,[26] which might be responsible for the minute weight loss observed between 200 and 260 °C. The weight loss between ~260 °C and ~400 °C was attributed primarily to oxygen loss from $Li_{0.2}Ni_{0.5}Mn_{0.5}O_2$. The onset temperature of oxygen loss from $Li_{0.2}Ni_{0.5}Mn_{0.5}O_2$ is considerably higher, and the amount of oxygen loss up to 400 °C is much lower relative to those for $Li_{0.33}NiO_2$.[26] The large weight drop that began at ~400 °C was attributed to the decomposition of PVDF (10 wt % present in the electrode), which was noted in the

(47) *Mineral physics & crystallography: a handbook of physical constants*; American Geophysical Union: Washington, DC, 1995.
(48) Wang, L.; Maxisch, T.; Ceder, G. *Chem. Mater.* **2007**, *19*, 543.

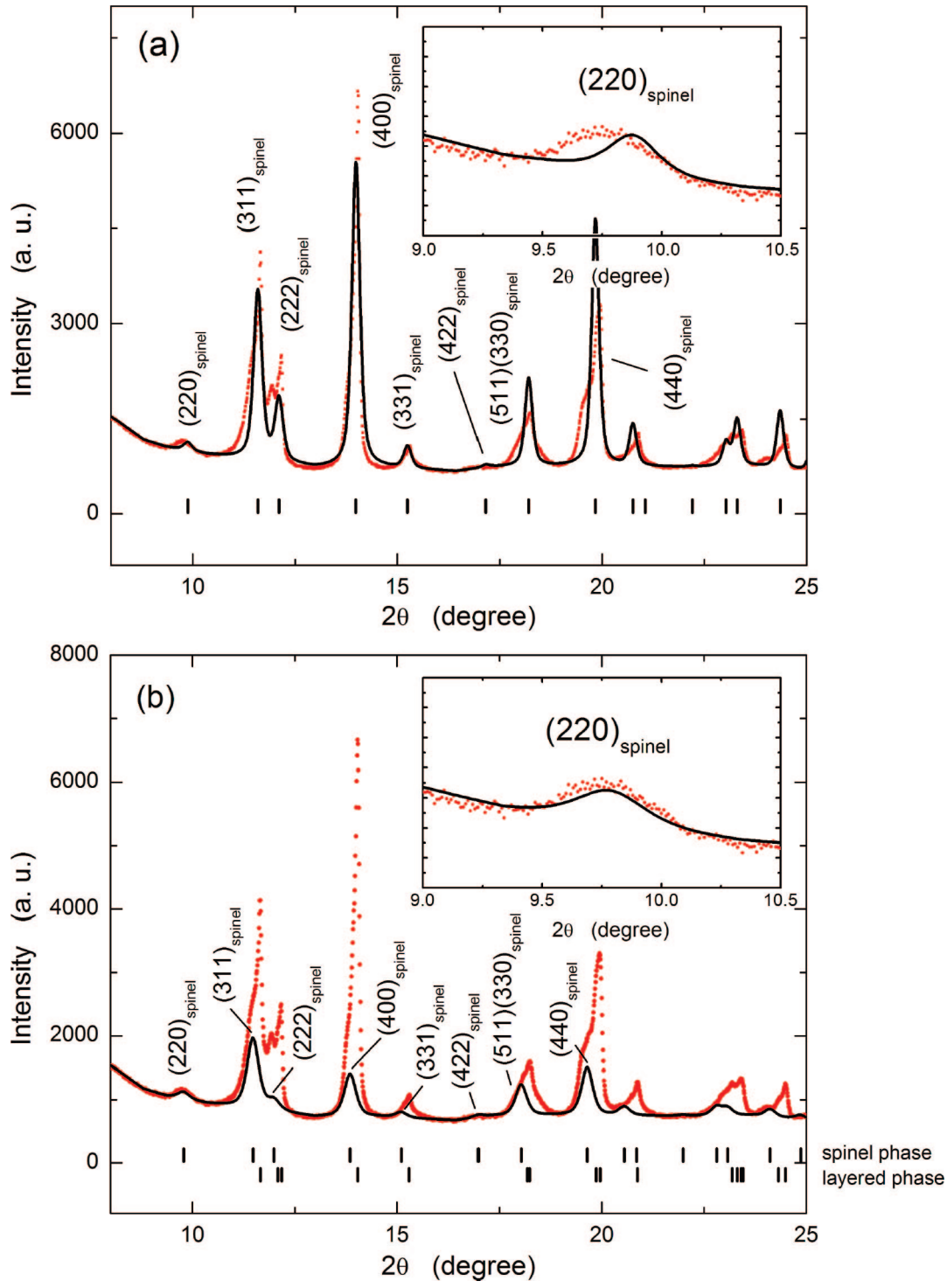

Figure 7. Phase analysis on the X-ray diffraction patterns of the charged $Li_{0.2}Ni_{0.5}Mn_{0.5}O_2$ obtained at 300 °C. (a) Single-phase spinel-type model and (b) two-phase model that consists of the spinel-type and rhombohedral phases. At this temperature, the spinel-type phase has larger lattice parameters ($a_{hex.}$ = 2.96 Å, $c_{hex.}$ = 14.49 Å in the hexagonal unit cell setting) and a large unit cell volume (110 Å^3) in comparison to those of the rhombohedral phase ($a_{hex.}$ = 2.89 Å, $c_{hex.}$ = 14.22 Å, and $V_{hex.}$ = 103 Å^3). The increase in the unit volume of the spinel-type phase (approximately 7% at 300 °C) relative to the rhombohedral structure in the charged electrode can be attributed to additional oxygen loss.

TGA data of the pristine $LiNi_{0.5}Mn_{0.5}O_2$ electrode (Supporting Information Figure S4). The onset temperature of weight loss and the amount of weight loss from discharged $Li_{0.9}Ni_{0.5}Mn_{0.5}O_2$ electrode were found comparable to pristine $LiNi_{0.5}Mn_{0.5}O_2$ electrode, which indicated that the oxygen loss from $Li_{0.9}Ni_{0.5}Mn_{0.5}O_2$ at temperatures lower than 400 °C was insignificant.

Discussion

Stability of the Rhombohedral Structure ($R\bar{3}m$). *Cation Migration in the Rhombohedral Structure (100−275 °C).* No change in the cation distribution of the charged and discharged samples is noted upon heating from RT to 100 °C. A considerable amount of cations migrates from the

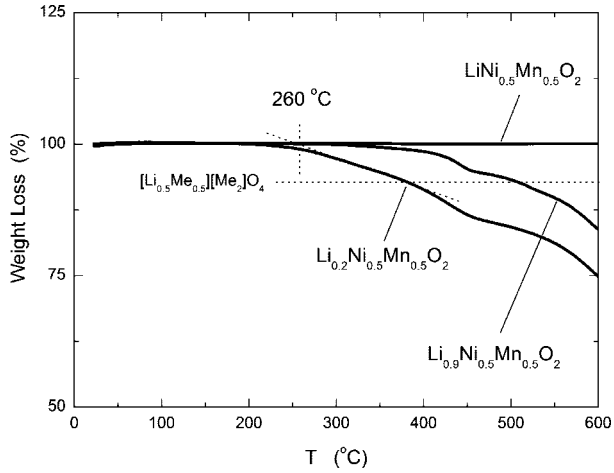

Figure 8. TGA curves of the pristine $LiNi_{0.5}Mn_{0.5}O_2$, charged $Li_{0.2}Ni_{0.5}Mn_{0.5}O_2$, and discharged $Li_{0.9}Ni_{0.5}Mn_{0.5}O_2$ under nitrogen gas flow in the temperature range of 25−600 °C. The pristine sample was measured without carbon and binder, and no weight change has been observed in this temperature range.

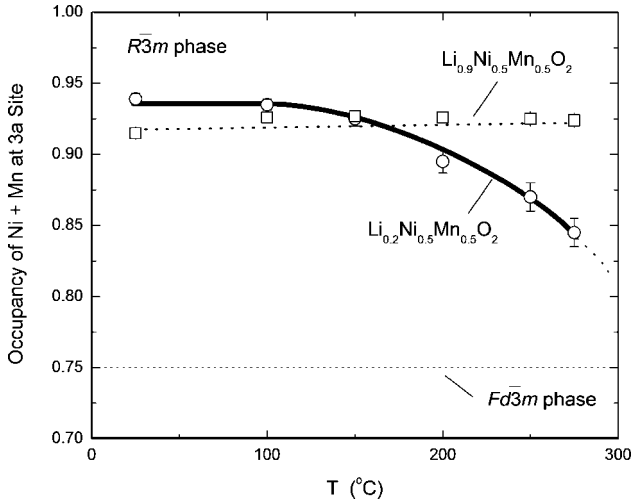

Figure 9. Change in the occupancy of Ni and Mn ions at the 3a site for $Li_{0.2}Ni_{0.5}Mn_{0.5}O_2$ (open circles) and $Li_{0.9}Ni_{0.5}Mn_{0.5}O_2$ (open squares) in the temperature range between 25 and 275 °C. The spinel structure ($Fd\bar{3}m$) can be presumed as the layered formulation, in which the occupancies of transition metals at 3a site (metal layer) and 3b site (lithium layer) are 0.75 and 0.25, respectively.

transition metal layer to the Li layer, and the occupancy of the 3a sites in the $Li_{0.2}Ni_{0.5}Mn_{0.5}O_2$ electrode gradually decreases from ~0.94 in $[\square_{0.74}Li_{0.2}Ni_{0.06}]_{3b}[\square_{0.06}Ni_{0.44}Mn^{4+}{}_{0.5}]_{3a}O_2$ at 100 °C to ~0.85 in $[\square_{0.65}Li_{0.2}Me_{0.15}]_{3b}[\square_{0.15}Me_{0.85}]_{3a}O_2$ per formula unit at 275 °C, as shown in Figure 9. As X-ray diffraction data in this temperature range did not show any evidence of long-range ordering at tetrahedral sites characteristic of the spinel structure, the cations found on the tetrahedral 6c sites by Rietveld analysis (~0.02 nickel per formula unit for all samples as shown in Table 1) were merged into the 3b site for simplicity in Figure 9. Cation migration from the octahedral 3a sites to 3b sites (there are three adjacent edge-shared octahedral sites in the Li layer for each 3a site) requires hopping through tetrahedral 6c sites in the lithium layer (face-shared with the 3a and 3b sites), as discussed previously[16,17,26] and shown in Figure 10. Since it is very difficult for Ni^{4+} and Mn^{4+} to occupy tetrahedral sites, it is postulated that low-spin Ni^{3+} ions ($t_{2g}{}^6 e_g{}^1$) in $Li_{0.2}Ni_{0.5}Mn_{0.5}O_2$ from the transition metal layer hop via tetrahedral sites ($e^4\ t_2{}^3$) into the Li layer upon heating. Further studies are needed to confirm this hypothesis.

The layered character of the rhombohedral structure ($R\bar{3}m$) can be stabilized by having high lithium contents in the lithium layer, as evidenced by a constant occupancy of the 3a sites in the discharged $Li_{0.9}Ni_{0.5}Mn_{0.5}O_2$ electrode upon heating to 275 °C (Figure 9). This is in good agreement with the fact that the $c_{hex.}/a_{hex.}$ ratio remains nearly constant up to 300 °C, as shown in Figure 6e. It is not understood if the difference in the extent of cation migration between the charged and the discharged samples at temperatures lower than 300 °C results from thermodynamic considerations or kinetic limitation. Previous first-principles calculations have suggested that all layered Li_xMeO_2 structures with space group $R\bar{3}m$ ($x < 1$) are metastable to spinel.[48,49] Cation migration, which is required for the spinel formation, can be facilitated by vacancies in the Li and transition metal layers at low temperatures. The number of vacancies in the Li and transition layers of $Li_{0.9}Ni_{0.5}Mn_{0.5}O_2$ is much lower (less than 0.10 at 3a and 3b sites per formula unit) than those of $Li_{0.2}Ni_{0.5}Mn_{0.5}O_2$, which may prohibit cation hopping from octahedral to tetrahedral sites and prevent cation migration within cubic-closed-packed oxygen array and the spinel formation.

Improved Stability of Rhombohedral $Li_xNi_{0.5}Mn_{0.5}O_2$ against Oxygen Loss. The change in the ratio of $c_{hex.}/a_{hex.}$ of the rhombohedral $Li_{0.2}Ni_{0.5}Mn_{0.5}O_2$ structure (Figure 6b) is attributed to gradual cation migration from the transition metal layer to the Li layer upon heating. The increase in the unit volume of $Li_{0.2}Ni_{0.5}Mn_{0.5}O_2$ is comparable to that of pristine $LiNi_{0.5}Mn_{0.5}O_2$ (Figure 6c,f), and TGA data show negligible weight loss at temperatures below 275 °C. Therefore, it is postulated that oxygen loss from the rhombohedral structure is minimal upon heating to ~275 °C, during which transition metal ions migrate to the lithium layer to form a disordered rhombohedral structure ($R\bar{3}m$). The rhombohedral to the spinel-type phase transition occurs between 275 and 300 °C, and the unit cell volume of the spinel-type phase is considerably larger than that of the rhombohedral phase, which suggests that oxygen loss from $Li_{0.2}Ni_{0.5}Mn_{0.5}O_2$ occurs at ~275 °C. This hypothesis is further supported by the TGA result, where the onset of weight loss in the $Li_{0.2}Ni_{0.5}Mn_{0.5}O_2$ electrode (a weight loss of 1 wt % relative to the pristine $LiNi_{0.5}Mn_{0.5}O_2$ electrode) occurs at ~260 °C (Figure 8 and Supporting Information Figure S4). The onset temperature of oxygen loss found in this study is in excellent agreement with that of heat release (~275 °C) from prior DSC measurements of $Li_{0.25}[Ni_{0.5}Mn_{0.5}]O_2$[12] (in the presence of electrolyte). It is surprising to note that oxygen loss from $Li_{0.2}Ni_{0.5}Mn_{0.5}O_2$ found in this study occurs at a considerably lower temperature than 340 °C reported previously from X-ray powder diffraction in the presence of electrolyte,[31] particularly considering that (1) similar heating rates were used and (2) electrolyte presence may reduce the onset temperature.

The stability of $Li_{0.2}Ni_{0.5}Mn_{0.5}O_2$ is remarkable in comparison to $Li_{0.3}Ni_{1.02}O_2$[26], where oxygen loss from bulk begins

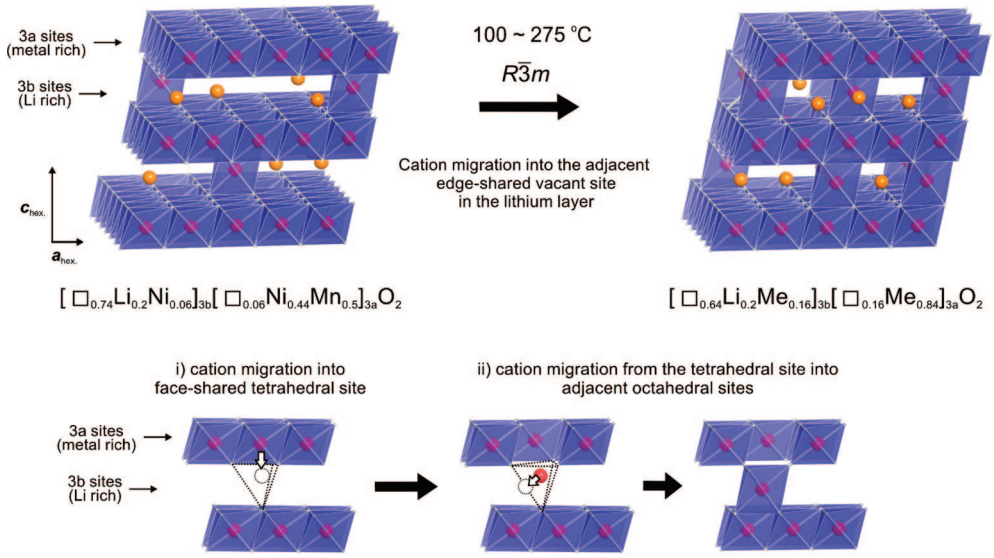

Figure 10. Schematic illustrations of the phase transition from the rhombohedral structure at 25 °C to the spinel-type phase observed at 275 °C. For $Li_{0.2}Ni_{0.5}Mn_{0.5}O_2$, cation mixing progresses between 3a and 3b sites during heating, leading to the formation of the pseudospinel structure (partial occupation of cations at 16d octahedral sites as a spinel phase), while for $Li_{0.9}Ni_{0.5}Mn_{0.5}O_2$, cation displacement was not confirmed until 275 °C. Cations, presumably Ni^{3+} ions, migrate from the octahedral sites in the metal layer to the octahedral sites in the lithium layer via face-shared tetrahedral site in the lithium layer.

at ~180 °C upon conversion of the layered structure ($R\bar{3}m$) to a pseudospinel structure (such as $Li_{0.68}Ni_{2.32}O_4$[27]). Oxygen loss from rhombohedral $Li_{0.2}Ni_{0.5}Mn_{0.5}O_2$ occurs at temperatures ~100 °C higher than that from $Li_{0.3}Ni_{1.02}O_2$.[27] The improved thermal stability of the rhombohedral $Li_{0.2}Ni_{0.5}Mn_{0.5}O_2$ phase may be attributed to the existence of Mn^{4+} ions (50% of transition metal ions) in the structure as oxygen loss from $Mn^{4+}O_2$ begins at ~300 °C in argon.[25,50] Excellent stability of $Li_xNi_{0.5}Mn_{0.5}O_2$ electrodes upon cycling to ~5 V reported recently[17] can be attributed to the intrinsic stability of rhombohedral $Li_xNi_{0.5}Mn_{0.5}O_2$ against oxygen loss, particularly at low lithium contents. The thermal stability of the rhombohedral $Li_xNi_{0.5}Mn_{0.5}O_2$ structure can be improved by increasing its lithium content, which is shown previously in Li_xNiO_2.[25,26,29] The onset temperature of decomposition to the spinel-type phase is shifted to a higher temperature (~350 °C) in $Li_{0.9}Ni_{0.5}Mn_{0.5}O_2$ relative to that of $Li_{0.2}Ni_{0.5}Mn_{0.5}O_2$ (~275 °C). This is further supported by the TGA result that the oxygen loss from $Li_{0.9}Ni_{0.5}Mn_{0.5}O_2$ at temperatures lower than 400 °C was minimal (<1 wt % relative to that of pristine $LiNi_{0.5}Mn_{0.5}O_2$ electrode).

Thermal Decomposition of $Li_xNi_{0.5}Mn_{0.5}O_2$. Structural changes of $Li_{0.2}Ni_{0.5}Mn_{0.5}O_2$ and $Li_{0.9}Ni_{0.5}Mn_{0.5}O_2$ upon heating from RT to 600 °C in argon are shown in Figure 11a,b, respectively. In this section, we discuss the formation of the spinel-type and rocksalt-type structures upon oxygen loss from the rhombohedral structure.

Transition from the Rhombohedral ($R\bar{3}m$) *to Spinel-Type* ($Fd\bar{3}m$) *Structure (~275−450 °C).* It is proposed that the phase transition from the rhombohedral structure to the spinel-type structure in $Li_{0.2}Ni_{0.5}Mn_{0.5}O_2$ can be written as

$$[\square_{0.64}Li_{0.2}Me_{0.16}]_{3b}[\square_{0.16}Me_{0.84}]_{3a}O_2 \rightarrow 0.5(1-y)[Li_{0.4/(1-y)}Me_{2y/(1-y)}]_{8a}[Me_2]_{16d}O_4 + yO_2\uparrow \quad (3)$$

where y represents the extent of oxygen loss relative to $Li_{0.2}Ni_{0.5}Mn_{0.5}O_2$ upon conversion to the spinel-type structure. The value of y may vary between 0 and 0.2. When y is equal to 0.2, oxygen loss associated with the formation of the spinel-type phase is ~7 wt %. This is in good agreement with the fact that the weight loss of $Li_{0.2}Ni_{0.5}Mn_{0.5}O_2$ electrode is ~8 wt % relative to pristine $Li_{0.2}Ni_{0.5}Mn_{0.5}O_2$ electrode at 400 °C (Figure 8), where the spinel-type phase becomes the dominant phase (Figure 4a and Figure 6).

Detailed stoichiometries and cation distributions of the spinel-type structure at different temperatures are not known. Comparison of observed lattice parameters of the spinel-type structure in Figure 6 with those of known spinel compounds may provide some insights to the average valence of transition metal ions, the extent of oxygen loss in the spinel-type structure, and the cation distributions. The lattice parameter, a_{spinel}, of the spinel-type phase found in the charged sample at 400 °C is equal to 8.36 Å, which is comparable to that of $NiMn_2O_4$ (a_{spinel} = 8.39 Å at RT; 8.42 Å at 400 °C; the average valence of transition metals = 2.7)[51,52] but considerably larger than that of $LiNi_2O_4$ (a_{spinel} = 8.04 Å at RT),[28] $LiNi_{0.5}Mn_{1.5}O_4$ (a_{spinel} = 8.17 Å at RT)[53] and $LiMn_2O_4$ (a_{spinel} = 8.24 Å at RT)[54] having average transition metal valence of 3.5. This comparison further supports that the spinel-type structure in the charged sample at 400 °C may have y values close to 0.2, having a chemical formula of $[Li_{0.5}Me_{0.5}]_{8a}[Me_2]_{16d}O_4$ (with a valence state of 3+) provided that all the Li ions are located on the tetrahedral 8a sites. As the intensities of the $(220)_{spinel}$ and $(422)_{spinel}$ reflections of the spinel-type phase are clearly visible in

(49) Van der Ven, A.; Ceder, G. *Phys. Rev. B* **1999**, *59*, 742.
(50) Schilling, O.; Dahn, J. R. *J. Electrochem. Soc.* **1998**, *145*, 569.
(51) Gillot, B.; Baudour, J. L.; Bouree, F.; Metz, R.; Legros, R.; Rousset, A. *Solid State Ionics* **1992**, *58*, 155.
(52) Brabers, V. A. M.; Terhell, J. *Phys. Status Solidi A* **1982**, *69*, 325.
(53) Ariyoshi, K.; Iwakoshi, Y.; Nakayama, N.; Ohzuku, T. *J. Electrochem. Soc.* **2004**, *151*, A296.
(54) Ohzuku, T.; Kitagawa, M.; Hirai, T. *J. Electrochem. Soc.* **1990**, *137*, 769.

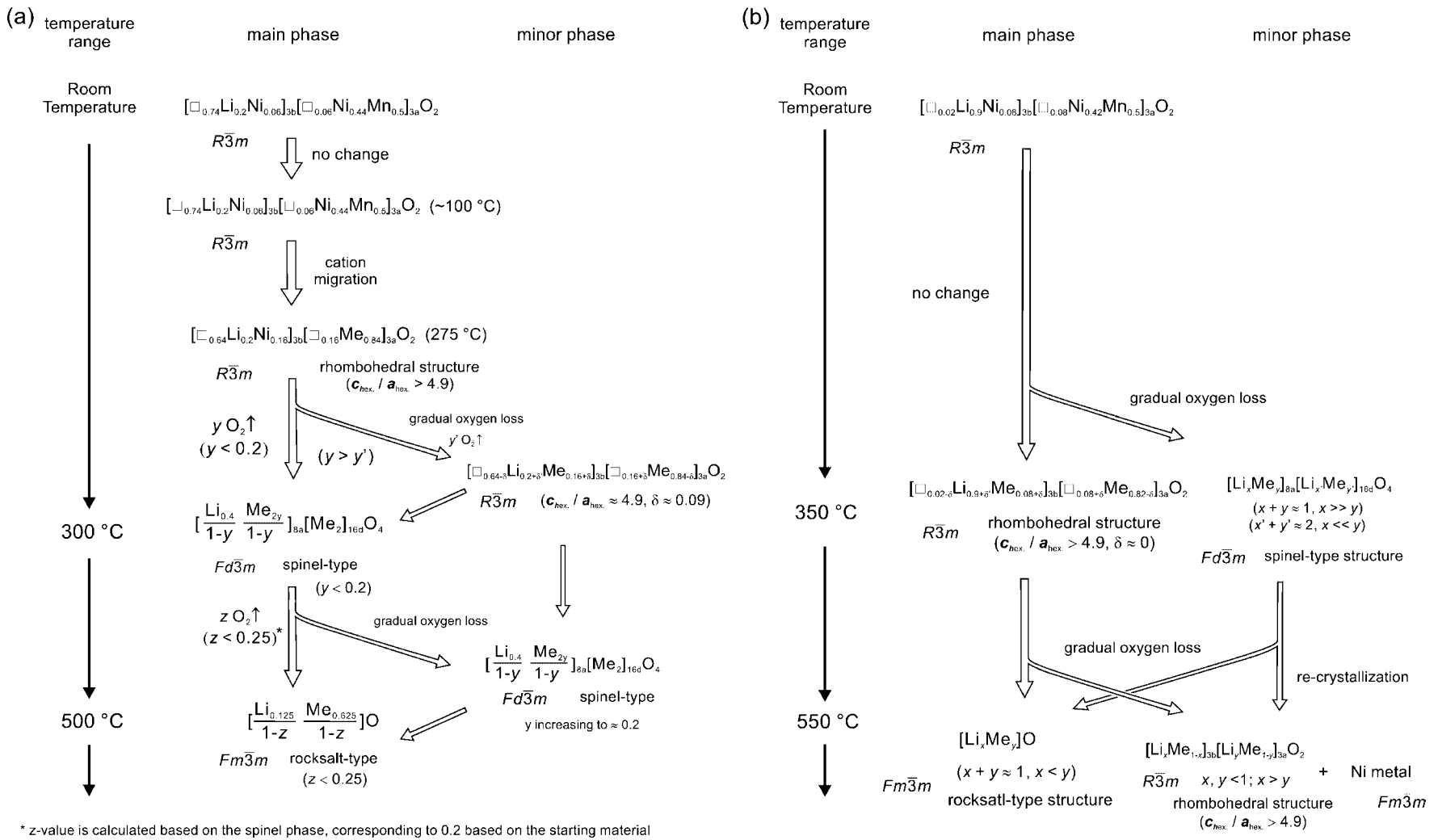

Figure 11. Schemes on the thermal decomposition mechanisms of (a) $Li_{0.2}Ni_{0.5}Mn_{0.5}O_2$ and (b) $Li_{0.9}Ni_{0.5}Mn_{0.5}O_2$ during heating up from 25 to 600 °C in argon in absence of electrolyte.

Figure 7 (transition metals most likely present on the 8a sites, the formation of stoichiometric $[Li]_{8a}[Me_2]_{16d}O_4$ analogous to $[Li]_{8a}[Ni_2]_{16d}O_4$ as suggested for the thermal decomposition of Li_xNiO_2[48] is unlikely upon heating of $Li_{0.2}Ni_{0.5}Mn_{0.5}O_2$ in this study. This is in agreement with a recent study of nuclear magnetic resonance,[55] where thermally treated $Li_{0.5}NiO_2$ has a cation distribution significantly different from the ideal $LiNi_2O_4$ spinel structure. The spinel-type phase is stabilized over a much wider temperature window (~300−600 °C) against conversion to the rocksalt-type phase upon heating of $Li_{0.2}Ni_{0.5}Mn_{0.5}O_2$ relative to $Li_{0.3}NiO_2$ (Figure 11a and Supporting Information Figure S5). The increased stability of the spinel-type structure is consistent with the observation that oxygen loss from $Li_{0.2}Ni_{0.5}Mn_{0.5}O_2$ is considerably smaller than that from $Li_{0.3}NiO_2$ for a given elevated temperature. It is postulated that the spinel-type structure, having a chemical formula of $[Li_{0.4/(1-y)}Me_{2y/(1-y)}]_{8a}[Me_2]_{16d}O_4$ (the extent of oxygen loss, $y > 0$), may consist of Mn^{3+} that can disproportionate into Mn^{2+} and Mn^{4+}.[21] The Mn^{2+} ions can occupy the tetrahedral sites and stabilize the spinel-type structure against further oxygen loss and conversion to the rocksalt-type phase upon heating to higher temperatures. This hypothesis is supported by the existence of many thermodynamically stable Mn and/or Ni spinel compounds such as Mn_3O_4[56] and $NiMn_2O_4$,[52] in which (divalent) manganese ions are located at the tetrahedral sites.

Similar lattice parameters (a_{spinel} = 8.35−8.40 Å) were found for the spinel-type phase in the discharged and charged samples. Therefore, it is believed that the spinel-type structure in the discharged sample may have similar valence state of transition metal ions to that in the charged sample. Although the spinel-type phase becomes noticeable at ~400 °C, the rhombohedral phase exists as the major phase in the discharged sample at temperatures lower than 550 °C. This is in contrast to thermal decomposition of the charged sample, which has the spinel-type structure as the major phase in the temperature range from 400 to 550 °C (Figure 6).

Transition from the Spinel-Type ($Fd\bar{3}m$) to the Rocksalt-Type ($Fm\bar{3}m$) Structure (above ~500 °C). It is proposed that the phase transition from the spinel-type structure to the rocksalt-type structure in $Li_{0.2}Ni_{0.5}Mn_{0.5}O_2$ occurs when the extent of oxygen loss from bulk, y in $Li_{0.2}Ni_{0.5}Mn_{0.5}O_{2-2y}$ or $[Li_{0.4/(1-y)}Me_{2y/(1-y)}]_{8a}[Me_2]_{16d}O_4$ approaches 0.2. This formation of the rocksalt-type structure can be written as:

$$0.5[Li_{0.5}Me_{0.5}]_{8a}[Me_2]_{16d}O_4 \rightarrow (2-2z)[Li_{0.125/(1-z)}Me_{0.625/(1-z)}]O + zO_2 \quad (4)$$

where z represents the extent of additional oxygen loss relative to $Li_{0.2}Ni_{0.5}Mn_{0.5}O_{2-2y}$ (y = ~0.2) (or $[Li_{0.5}Me_{0.5}]_{8a}[Me_2]_{16d}O_4$ having all lithium ions on the 8a sites) upon conversion to the rocksalt-type structure. The value of z may vary from 0 to 0.25. When $z = 0.25$, the rocksalt-type phase may be formulated as $[Li_{0.167}Me_{0.833}]O$, in which the average oxidation number of transition metals is calculated to be 2.2+. When z is equal to 0.25, oxygen loss associated with the formation of the rocksalt-type phase is ~14 wt % based on the $Li_{0.2}Ni_{0.5}Mn_{0.5}O_2$ electrode. This is in good agreement with the fact that the weight loss of $Li_{0.2}Ni_{0.5}Mn_{0.5}O_2$ electrode is ~11.5 wt % relative to pristine $Li_{0.2}Ni_{0.5}Mn_{0.5}O_2$ electrode at 600 °C (Figure 8 and Supporting Information Figure S4), at which temperature the rocksalt-type phase becomes the dominant phase (Figure 4a and Figure 6) with the minor spinel-type phase. In addition, lattice parameter of the rocksalt-type phase, $a_{rocksalt}$, is 4.29 Å at 600 °C (Table 2), and it is comparable to that of $Ni_{0.5}Mn_{0.5}O$ ($a_{rocksalt}$ = 4.33−4.36 Å at 600 °C), which was estimated from the thermal expansion coefficients of NiO[43] and MnO[44] (Supporting Information Table S1). Having the similar unit cell dimension to rocksalt $Ni_{0.5}Mn_{0.5}O$ suggests that the rocksalt-type structure formed from $Li_{0.2}Ni_{0.5}Mn_{0.5}O_2$ at 600 °C may have a chemical formula close to $[Li_{0.167}Me_{0.833}]O$, which is likely to consist of Ni^{2+}, Mn^{2+}, Li^+, and Mn^{3+}.

The phase transitions found in $Li_{0.9}Ni_{0.5}Mn_{0.5}O_2$ at 600 °C are considerably different from those found for $Li_{0.2}Ni_{0.5}Mn_{0.5}O_2$. In addition to the rocksalt-type phase ($a_{rocksalt}$ = 4.32 Å) as the major phase, a new rhombohedral phase ($a_{hex.}$ = 2.91 Å and $c_{hex.}$ = 14.45 Å) and nickel metal (a_{cubic} = 3.55 Å) are present as minor phases. This new rhombohedral phase has lattice parameters similar to those of the pristine sample ($a_{hex.}$ = 2.91 Å and $c_{hex.}$ = 14.43 Å at 600 °C) and considerably different lattice parameters from those of the rhombohedral structure observed at temperatures below 550 °C, as shown in Figure 6d. It is postulated that the appearance of this new phase results from the recrystallization of the rhombohedral $LiNi_{0.5}Mn_{0.5}O_2$ structure at high temperatures. This observation is in good agreement with the recrystallization of $LiNiO_2$ upon thermal decomposition of Li_xNiO_2 when x is greater than or equal to 0.5.[29,48] It should be mentioned that the intensity of $(003)_{hex.}$ is relatively low relative to other reflections, which indicates that the recrystallized $LiNi_{0.5}Mn_{0.5}O_2$ structure has greater extent of interlayer mixing than the pristine sample. This observation is in good agreement with previous findings,[15] which reveal that the $LiNi_{0.5}Mn_{0.5}O_2$ samples synthesized at 600 °C in air show considerable interlayer mixing (~0.16 per unit formula). Since the oxygen partial pressure is low in this experimental condition (an argon filled capillary), this recrystallization of the rhombohedral phase is accompanied with solid-state reduction of the spinel-type to the rocksalt-type phase and the formation of the Ni metal. The lattice parameter of Ni metal (a = 3.55 Å at 600 °C) is in good agreement with the reported values (a = 3.52 Å at 25 °C and 3.56 Å at 600 °C).[57] It is noted that the lattice parameter of the rocksalt-type phase found in the discharged sample is considerably larger than that in the charged sample. This difference may be related to the fact that the rocksalt-type phase in the discharged sample has a higher concentration of Mn ions than that in the charged sample.

Comparison with Previously Proposed Decomposition Mechanisms of Li_xNiO_2-Based Oxides. As shown in Figure

(55) Chazel, C.; Menetrier, M.; Carlier, D.; Croguennec, L.; Delmas, C. *Chem. Mater.* **2007**, *19*, 4166.
(56) Goodenough, J. B.; Loeb, A. L. *Phys. Rev.* **1955**, *98*, 391.
(57) Owen, E. A. Y., E. L. *Philos. Mag.* **1936**, *21*, 809.

11a,b, the proposed decomposition mechanism of $Li_{0.2}Ni_{0.5}Mn_{0.5}O_2$ and $Li_{0.9}Ni_{0.5}Mn_{0.5}O_2$ in this study includes cation migration in the rhombohedral structure, conversion to the spinel-type structure and coexistence of the rhombohedral and spinel-type structures, and conversion to the rocksalt-type structure and coexistence of the spinel-type and rocksalt-type structures. The proposed mechanism is similar to that reported previously for Li_xNiO_2[26,27] (shown in Supporting Information Figure S5), but one difference is noted. Previous studies[26,27] have proposed a phase transition from the spinel-type (pseudospinel) to the disordered rhombohedral structure. However, this phase transition is not found (Figure 11a); in contrast, it is shown in this study that cation migration occurs and the interlayer mixing increases in the rhombohedral structure at temperatures greater than ~100 °C, and the rhombohedral phase in $Li_{0.2}Ni_{0.5}Mn_{0.5}O_2$ gradually loses oxygen at temperatures higher than ~275 °C and disappears at ~450 °C. It should also be mentioned that several previous studies[29,48] have suggested that Li_xNiO_2 decomposes into spinel $LiNi_2O_4$ and rhombohedral $LiNiO_2$ when x is greater than 0.5 and into spinel $LiNi_2O_4$, rocksalt NiO, and O_2 when x is less than 0.5 upon heating. However, these decomposition processes, specifically stoichiometric spinel $[Li]_{8a}[NiMn]_{16d}O_4$ and pristine rhombohedral $[Li]_{3b}[Ni_{0.5}Mn_{0.5}]_{3a}O_2$ structures, are not found upon heating of $Li_{0.2}Ni_{0.5}Mn_{0.5}O_2$ and $Li_{0.9}Ni_{0.5}Mn_{0.5}O_2$ (without electrolyte) to 600 °C in argon in this study (Figure 11a,b).

Conclusions

Thermal instability of cycled $Li_{0.2}Ni_{0.5}Mn_{0.5}O_2$ and $Li_{0.9}Ni_{0.5}Mn_{0.5}O_2$ electrodes has been examined by in situ synchrotron X-ray diffraction and TGA measurements upon heating from RT to 600 °C in argon (in absence of electrolyte). This study shows that $Li_xNi_{0.5}Mn_{0.5}O_2$ has thermal stability superior to other Li_xNiO_2-related materials by comparing X-ray diffraction and TGA data collected under similar experimental conditions. We note the following: (1) a higher onset temperature of oxygen release (occurring at ~275 °C for $Li_{0.2}Ni_{0.5}Mn_{0.5}O_2$, ~100 °C higher than those of $Li_{0.3}NiO_2$ and ~40 °C higher than $Li_{0.3}Ni_{0.7}Co_{0.15}Al_{0.15}O_2$[26,27]) as a result of increased stability of the disordered rhombohedral structure and (2) reduced oxygen loss as a result of the increased stability of the spinel-type phase (partly retained at 600 °C) against oxygen loss to form the rocksalt-type phase upon heating to 600 °C. The information not only allows the comparison of intrinsic thermal stability of different electrode materials but also provides new insights to the origin of the electrochemical behavior of $Li_xNi_{0.5}Mn_{0.5}O_2$ and design of new electrode materials with increased thermal stability. For example, the intrinsic stability of rhombohedral $Li_xNi_{0.5}Mn_{0.5}O_2$ structure at very low Li contents against oxygen loss is believed key to the good cyclability of $Li_xNi_{0.5}Mn_{0.5}O_2$ electrodes to high voltages such as ~5 V.[17] It should be mentioned that the onset temperature of thermal decomposition and decomposition products from $Li_xNi_{0.5}Mn_{0.5}O_2$ electrodes in this study can be used to compare with those of other materials measured under similar conditions to show relative thermal stability and understand stability origin of materials. However, as the thermal decomposition of electrodes can be dependent on the oxygen partial pressure (argon filled capillaries vs practical Li batteries) and heating rates (controlled heating or abuse battery testing), care should be taken in the direct comparison of thermal decomposition products found in abused lithium batteries and those reported in this study.

Acknowledgment. This work was financially supported in part by the Office of Naval Research Young Investigator Award N00014-03-10448, the MRSEC Program of the National Science Foundation under award number DMR 02-13282, and a 2006 Air Products Faculty Excellence Award. The synchrotron diffraction experiments work was made possible through the support of the Japanese Ministry of Education, Science, Sports and Culture, Nanotechnology Support Project (Proposal No. 2006B1589/BL02B2) with the approval of Japan Synchrotron Radiation Research Institute (JASRI). The authors thank S. Kumar for preparing cycled $Li_xNi_{0.5}Mn_{0.5}O_2$ electrodes and K. Kato and K. Osaka from SPring-8 and T. Mitani, T. Ooi, and T. Sasaki from JAIST for their kind help with the synchrotron radiation experiments. The authors are also indebted to J. Breger and C.P. Grey for providing some pristine $LiNi_{0.5}Mn_{0.5}O_2$ samples used in this study. Figures 5 and 8 were drawn with VICS-II software developed by K. Momma and F. Izumi.

Supporting Information Available: Change in lithium−oxygen and metal−oxygen bond lengths on the pristine sample as a function of the temperature, change in the unit cell volume on the pristine $LiNi_{0.5}Mn_{0.5}O_2$ sample as a function of temperature, structural analysis by the Rietveld method, thermogravimetric curves, scheme on the thermal degradation process for $Li_{0.3}NiO_2$, and crystallographic parameters of oxides and metals as reference materials (PDF). This material is available free of charge via the Internet at http://pubs.acs.org.

CM800314D